Low-Temperature Preparation of Tailored Carbon Nanostructures in Water

Supporting Information

Ruth Szilluweit,[1,†] Tobias N. Hoheisel,[1,2,†] Martin Fritzsche,[1] Bernt Ketterer,[3] Anna Fontcuberta i Morral,[3]

Davide Demurtas,[4] Vincent Laporte,[5] René Verel,[2] Sreenath Bolisetty,[6] Raffaele Mezzenga,[6] and Holger Frauenrath[1,]*

[1] Ecole Polytechnique Fédérale de Lausanne (EPFL)
Institute of Materials
Laboratory of Macromolecular and Organic Materials

EPFL – STI – IMX – LMOM, MXG 037, Station 12
1015 Lausanne, Switzerland

holger.frauenrath@epfl.ch

[2] ETH Zürich, Switzerland
Department of Materials

[3] Ecole Polytechnique Fédérale de Lausanne (EPFL), Switzerland
Institute of Materials
Laboratory of Semiconducting Materials

[4] Ecole Polytechnique Federale de Lausanne (EPFL)
Interdisciplinary Centre for Electron Microscopy
Bio-EM Analysis

[5] Ecole Polytechnique Federale de Lausanne (EPFL)
Interdisciplinary Centre for Electron Microscopy
Surface Analysis Facility

[6] ETH Zürich, Switzerland
Department of Agricultural and Food Sciences
Laboratory of Food and Soft Materials

[†] both authors contributed equally to this publication

Table of Contents

1. Supplementary Figures S1–S13

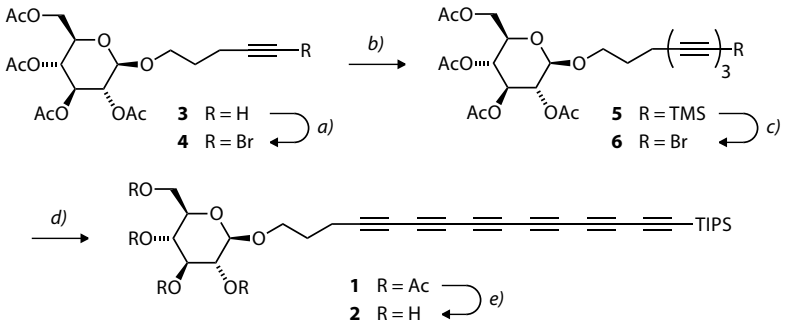

Supplementary Figure S1. The glycosylated hexa(ethynylene) amphiphile **2** was synthesized on the multi-gram scale in five steps starting from 4-pentyn-1-yl glucoside **3**. Thus, the repetitive sequential bromination[1,2] and Pd-catalyzed elongation of the oligo(ethynylene) moiety[3,4] afforded the acetylated hexa(ethynylene) **1** in 32% isolated yield over four steps (see also Supplementary Figure S2). Subsequent complete deacetylation of **1** then quantitatively furnished the hexa(ethynylene) **2** within minutes (see also Supplementary Figure S3). *Reagents and conditions: a)* $AgNO_3$, NBS, MeCN, 93%; *b)* 1,4-bis(trimethylsilyl)buta-1,3-diyne **7**, MeLi · LiBr, $ZnCl_2$, $PdCl_2$(dppf) · DCM, THF/toluene, 77%; *c)* AgF, NBS, MeCN, 81%; *d)* 1-triisopropylsilyl-6-trimethylsilylhexa-1,3,5-triyne **8**, MeLi · LiBr, $ZnCl_2$, $PdCl_2$(dppf) · DCM, THF/toluene, 55%; *e) i)* NaOMe, 1,4-dioxane, MeOH, *ii)* Amberlite IR-120 (H^+), 100%. For detailed experimental procedures as well as complete analytical data of all compounds, see the Experimental Part and the NMR Spectra Appendix (Sections 2 and 3 of the Supplementary Online Material).

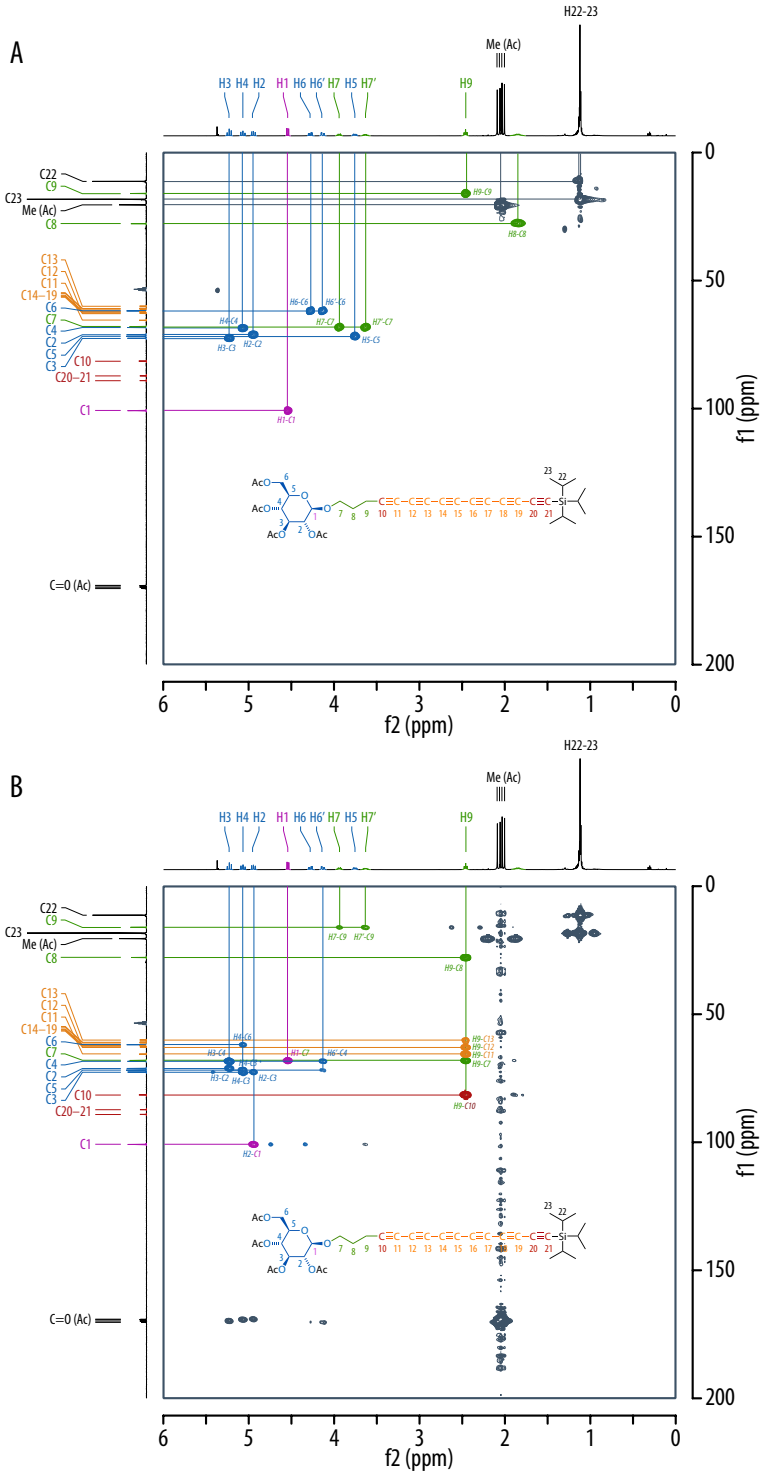

Supplementary Figure S2. 2D NMR spectra (400 MHz, CD_2Cl_2) of the protected, non-amphiphilic hexa(ethynylene) **1**. The combination of *A)* heteronuclear single-quantum correlation (HSQC) and *B)* heteronuclear multiple-bond correlation (HMBC) spectra allowed to assign the ^{13}C signals of 3 terminal acetylene carbons (red), the remaining 9 internal acetylene carbons (orange), the anomeric carbon of the carbohydrate head group (C1, purple), the other 5 carbohydrate carbons (C2–C6, blue), and the 3 carbons of the propyl spacer (C7–C9, green). For further analytical data of **1** and **2**, see the Experimental Part and the NMR Spectra Appendix (Sections 2 and 3 of the Supplementary Online Material).

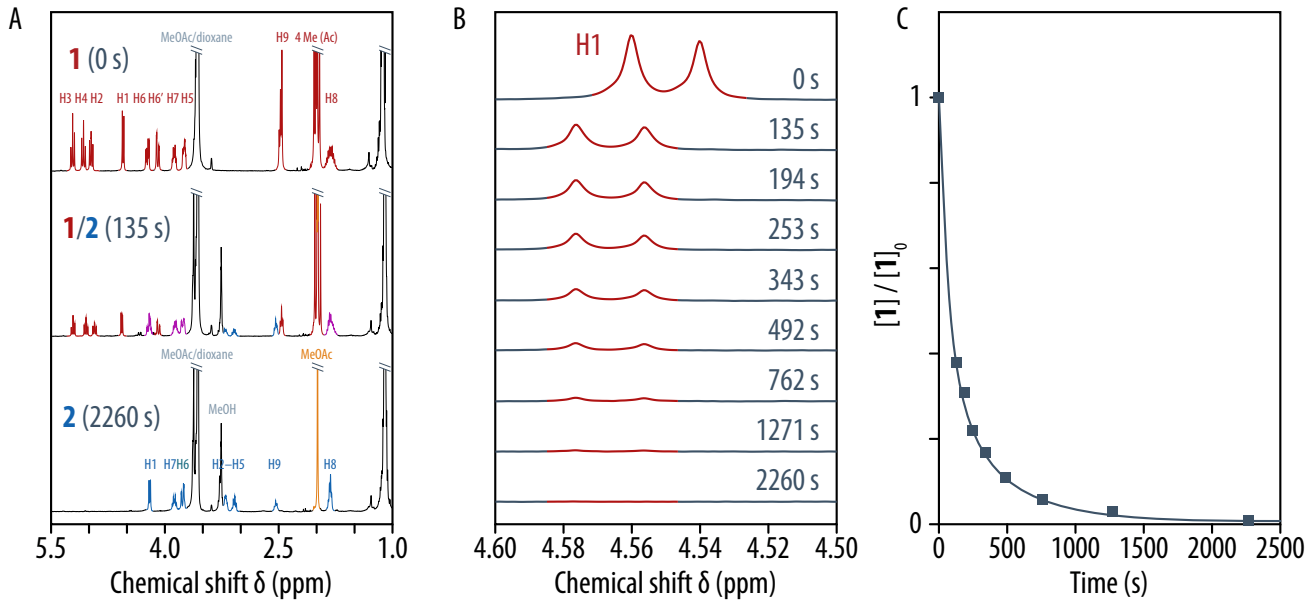

Supplementary Figure S3. *A)* ^{1}H NMR spectra (1,4-dioxane-d_8/CD_3OD) as a function of reaction time during the deacetylation of **1** catalyzed by NaOMe at room temperature clearly show the complete disappearance of ^{1}H resonances of **1** over 30–45 min to yield pure **2**. *B,C)* For diagnostic purposes, the ^{1}H NMR of the anomeric C*H* of **1** was used to follow the progress of the reaction. For reaction conditions as well as the complete analytical data of **2**, see Experimental Part and the NMR Spectra Appendix (Sections 2 and 3 of the Supplementary Online Material).

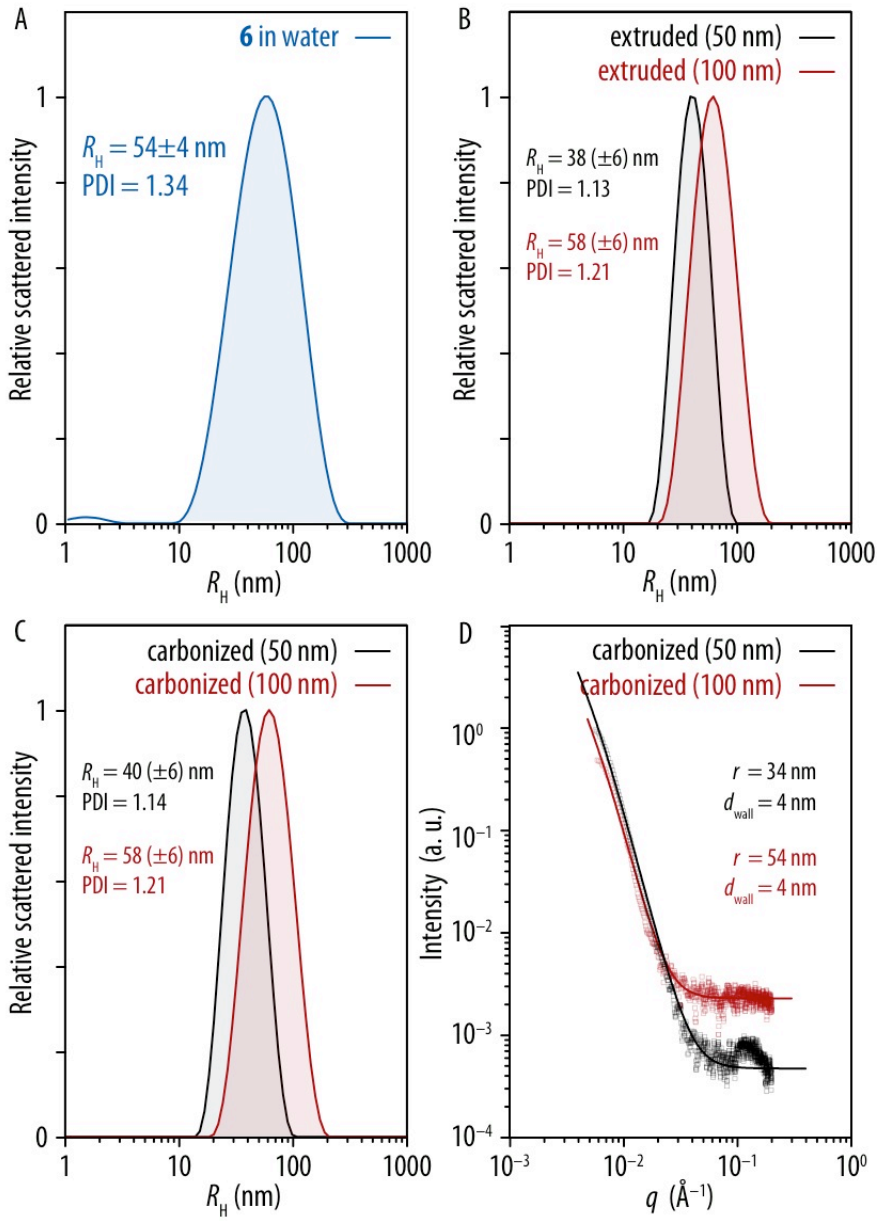

Figure S4. *A)* The DLS size distribution by intensity of aqueous dispersions of **2** as obtained upon injecting 200 μL of the stock solution of **2** into 800 μL of MilliQ water revealed the presence of colloidal aggregates with an average hydrodynamic radius of R_H = 54 (±4) nm and a polydispersity index (PDI) of 1.34. *B)* After extrusion of the dispersions through polycarbonate membranes with either 50 nm or 100 nm pore sizes, colloidal aggregates with controlled hydrodynamic radii of R_H = 38 (± 6) nm and 58 (± 6) nm and narrower size distributions (PDI of 1.13 and 1.21) were obtained. *C)* After carbonization by UV irradiation, the hydrodynamic radii and size distributions of R_H = 40 (± 6) nm (PDI 1.14) and 58 (± 6) nm (PDI 1.21) remained virtually unaffected. *D)* Small-angle X-ray scattering (SAXS) experiments on the two dispersions independently confirmed the DLS results and were consistent with the presence of hollow particles with a wall thickness of d_{wall} = 4 nm and total radii of r = 34 nm and 54 nm, respectively. For the respective cryo-TEM images, see Supplementary Figures S5 and S7. For detailed experimental procedures on dispersion preparation, DLS, and SAXS measurements, see Experimental Part (Section 2 of the Supplementary Online Material).

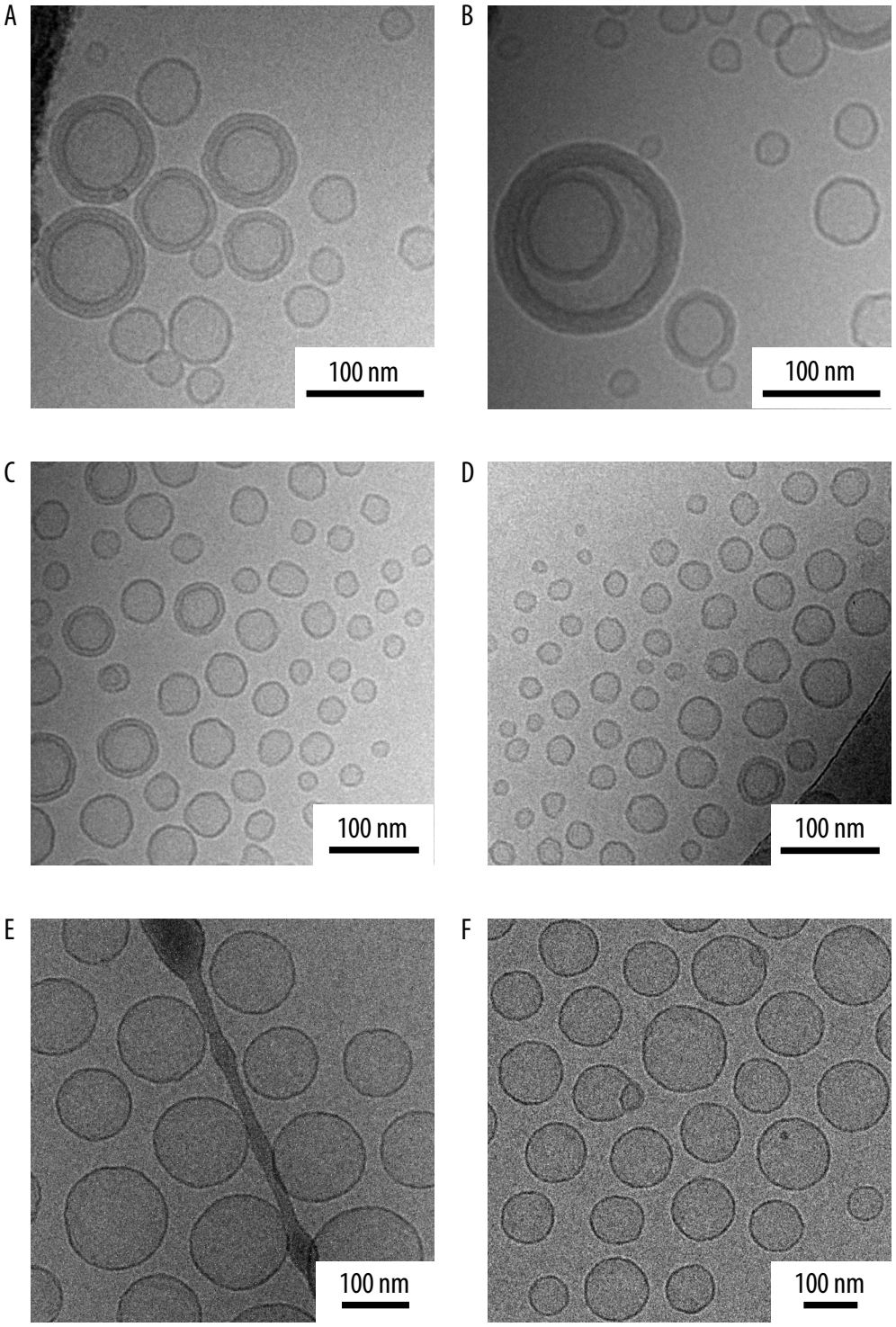

Supplementary Figure S5. Representative examples of cryo-TEM images of *A,B)* aqueous dispersions of **2** obtained by adding 200 μL of the stock solution of **2** (10 mg/mL, dioxane/MeOH 4:1) to 800 μL of MilliQ water revealed the presence of a mixture of unilamellar and multilamellar vesicles with diameters in the range of 20–140 nm. *C,D)* Extrusion of these dispersions through a polycarbonate membrane with 50 nm pore size yielded a dispersion of predominantly unilamellar vesicles with an average diameter of d = 43 nm (σ = 15 nm). *E,F)* Using a polycarbonate membrane with 100 nm pore size produced unilamellar vesicles with an average diameter of d = 104 nm (σ = 30 nm). In both cases, the vesicles were not perfectly spherical in shape but, in particular in the case of the smaller vesicles, revealed a tendency toward what appeared to be more 'polyhedral' shaped particles with 'flattened' vertices and kinks. For detailed experimental procedures on sample preparation and TEM imaging, see Experimental Part (Section 2 of the Supplementary Online Material).

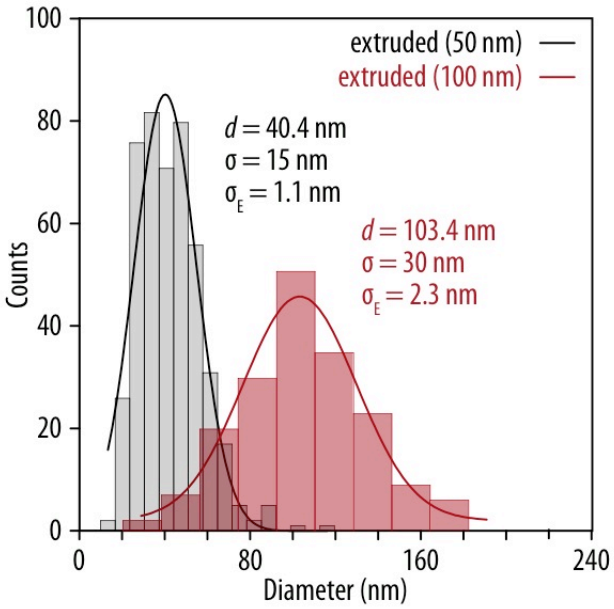

Supplementary Figure S6. Histograms of the size distributions of the vesicles in aqueous dispersions of **2** after extrusion through polycarbonate membranes with 50 nm (black) or 100 nm (red) pore sizes, as determined from cryo-TEM images (see Supplementary Figure S4 C,D for representative examples).

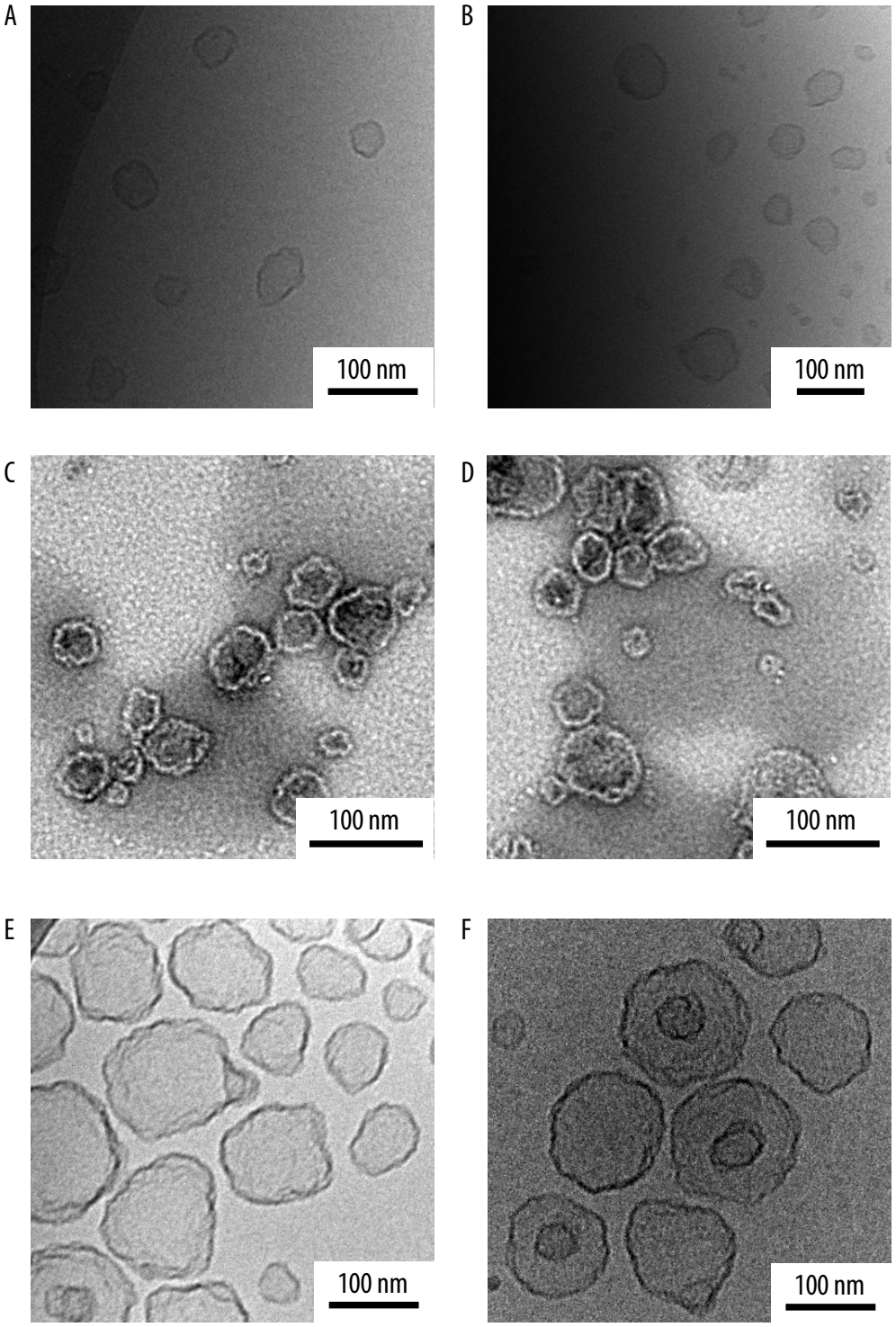

Supplementary Figure S7. Representative examples of cryo-TEM and TEM images of carbonized samples. *A,B)* Cryo-TEM images of aqueous dispersions of **2** after extrusion (50 nm) and UV irradiation (24 h, 1°C) showed 'irregularly' shaped hollow particles with rough walls and a 'polyhedral' morphology; however, the average diameter of the particles and their shell thickness were essentially preserved during the UV-induced carbonization. *C,D)* TEM images of these dispersions using uranyl acetate as a negative staining agent were consistent with the presence of hollow capsules. *E,F)* Cryo-TEM images of irradiated aqueous dispersions of **2** with larger vesicle size, obtained by extrusion (100 nm), exhibited similar, but larger capsules with the appropriate average diameters. For detailed experimental procedures on sample preparation and TEM imaging, see Experimental Part (Section 2 of the Supplementary Online Material).

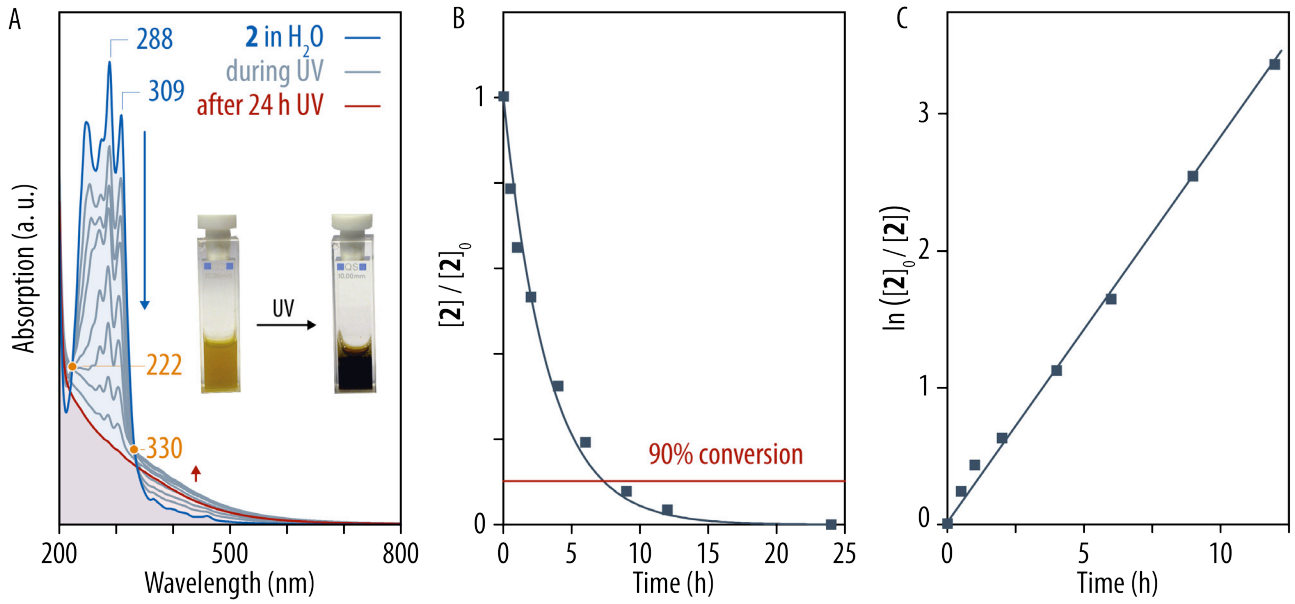

Supplementary Figure S8. *A)* UV/Vis spectra of aqueous dispersions of **2** after different times of UV irradiation showed that the absorption bands of the hexa(ethynylene) moieties successively decreased and eventually disappeared. The irradiated samples exhibited a broad and featureless absorption at wavelengths of up to 700 nm, presumably dominated by the increasing scattering of the dispersions of carbon nanoparticles. For the first seven UV/Vis spectra, recorded during the first 9 h of UV irradiation, two isosbestic points at 222 nm and 330 nm were observed, indicating that the underlying chemical reaction was, from a kinetic perspective, a simple two-state process. The subsequent deviation from these isosbestic points and overall decrease in intensity was probably due to gradual sedimentation of small amounts of material. Moreover, it is worth noting that any absorption bands in the range of 500–600 nm associated with the formation of a poly(diacetylene) were not observed at any stage of the carbonization process. Inset: sample vials of the dispersions before and after 6 h of UV irradiation, showing the color change from yellow to dark brown. *B)* A 'pseudo-kinetic' plot of $[A_{309,t} - (A_{400,t} \cdot A_{309,24h}/A_{400,24h})] / [A_{309,0} - (A_{400,0} \cdot A_{309,24h}/A_{400,24h})]$ as a proxy for normalized monomer consumption versus time fitted with a first-order exponential decay function, as well as *C)* a first-order plot of the same data indicated that, after a brief induction period with a higher reaction rate, the transformation roughly followed first-order kinetics.

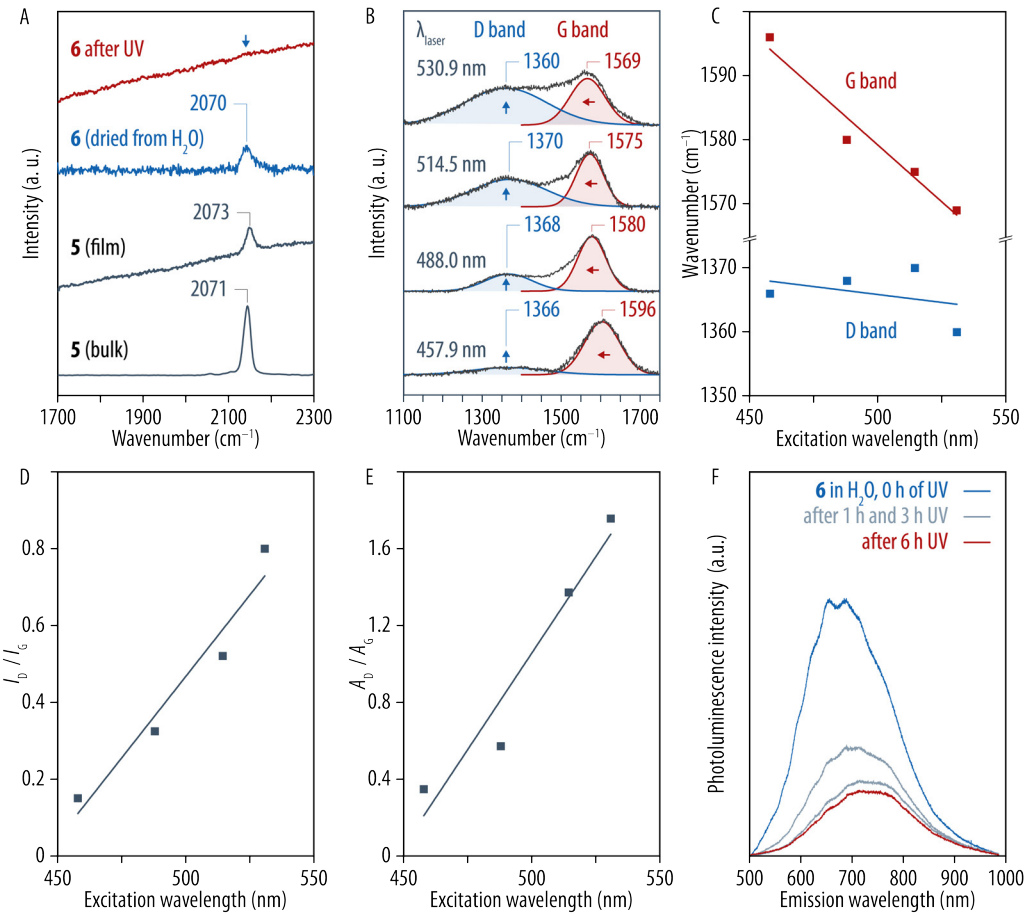

Supplementary Figure S9. *A)* Raman spectra of the dried carbonized material (obtained from dispersions of **2** after 24 h of UV irradiation at 1°C) in comparison to dried samples of **2** before UV irradiation as well as samples of the stable non-amphiphilic derivative **1** revealed that the hexa(ethynylene) Raman band at about 2070 cm^{-1} had completely disappeared. *B)* Background-corrected Raman spectra of the carbonized material exhibited the D and G band characteristic for bonds involving sp^2 hybridized carbon atoms in amorphous carbon materials. *C)* From the positions of the G band (1575 cm^{-1} at a laser excitation wavelength λ_{ex} = 514.5 nm) and the D band (1370 cm^{-1} at λ_{ex} = 514.5 nm), one may conclude that the carbon microstructure resembled the one of typical 'graphite-like' amorphous carbon (GLC, GLCH) that is located between nanocrystalline graphite (*nc*-*G*) and amorphous carbon (*a*-C, *a*-CH) on the disorder trajectory,[5,6] with an sp^3 content of about 10%. While the strong dispersion of the G band position with λ_{ex} (–0.35 cm^{-1}/nm) was consistent with the presence of significant amounts of hydrogenated carbons (as in *a*-CH), the independence of the D band position on λ_{ex} was in better agreement with nanocrystalline graphite (*nc*-*G*) and amorphous carbon (*a*-C) with a low hydrogen content (<15 at.%), as was *D,E)* the strong dependence of D and G peak intensity ratio I_D / I_G and peak area ratio A_D / A_G (and their values). The results may be attributed to the fact that the material contains hydrocarbon segments from the molecular precursors that remain unaffected by UV irradiation. *F)* The carbonized material exhibited photoluminescence at 500–1000 nm upon excitation at 488.0 nm, indicating the presence of hydrogenated carbon material, but the intensity actually decreased upon extended UV irradiation (the photoluminescence before UV irradiation was attributed to small amounts of prematurely carbonized material, also visible in the UV/Vis spectra; see Supplementary Figure S7), pointing at a progressive ordering of the carbon phase in the course of carbonization. Overall, the results of Raman spectroscopy suggested a complete conversion of the hexa(ethynylene)s and the formation of carbon material that closely resembled typical sp^2-rich amorphous carbons (*a*-C) obtained by, e.g., sputtering of a graphite target or by plasma-enhanced chemical vapor deposition after annealing of the deposited material at temperatures at or above 600°C (i.e., the onset of graphitization).[5,6]

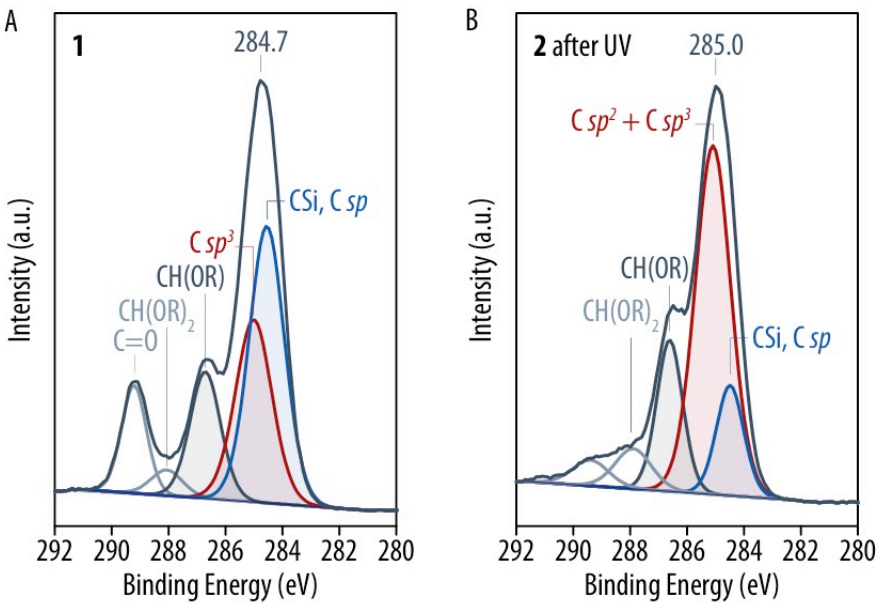

C1s peak (1)	Position (eV)	FWHM (eV)	Area (a. u.)	Concentration (at. %)
O=C–O	289.2	1.0	3800	11
O–C–O	288.1	1.3	1150	3
C–O	286.7	1.3	5500	16
C sp^3	285.0	1.5	9430	28
C sp + C–Si	284.6	1.4	13796	41

C1s peak (2 after UV)	Position (eV)	FWHM (eV)	Area (a. u.)	Concentration (at. %)
O=C–O	289.4	1.1	5194	4
O–C–O	287.9	1.5	16335	7
C–O	286.6	1.1	3972	18
C sp^3 + C sp^2	285.1	1.5	1926	57
C sp + C–Si	284.5	1.5	1234	14

Figure S10. X-ray photoelectron spectroscopy (XPS) and the results of peak deconvolution of *A)* the stable derivative **1** (top table) and *B)* a dried sample of a dispersion of **2** after UV irradiation (bottom table) were consistent with a conversion of the *sp* carbon atoms into a mixture of sp^2 and sp^3 hybridized carbon atoms. Thus, the envelope of the C1s peak in the XPS spectra of the carbon nanocapsules was shifted compared to the stable derivative **1**. The intensity of the peak attributed to the C *sp* (and C–Si) carbons was strongly reduced, while the intensity of the C sp^2 and C sp^3 band was significantly increased. Both XPS spectra were fitted with the same number of peaks and the same restrictions; the peak of the CH(OR) carbons (C2–C7) was used for calibration; peak deconvolution with separate C sp^2 and C sp^3 bands were not reproducible. While the peak deconvolution was not sufficiently reliable to draw definite conclusions, the conversion of acetylene carbons was estimated to be 60–90% from XPS data. It should be noted that XPS of the reactive amphiphile **2** (before UV irradiation) led to carbonization in the X-ray beam and was, hence, not used as a reference.

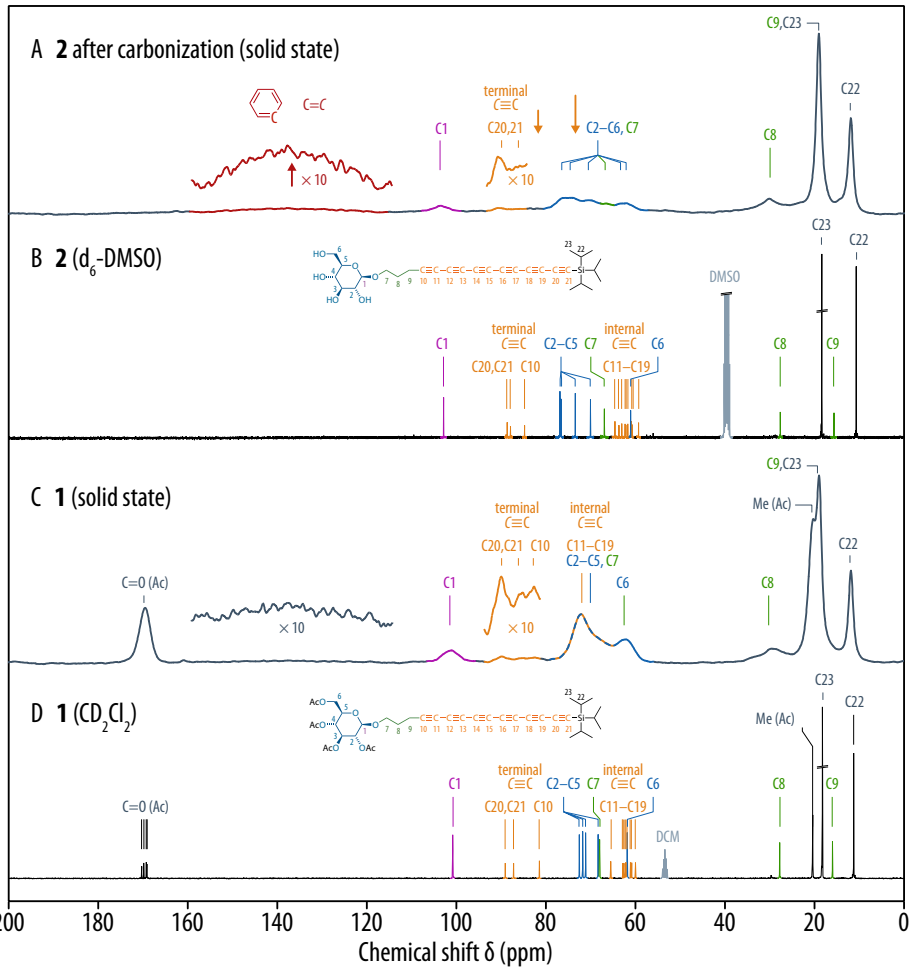

Figure S11. *A,C)* 700 MHz solid-state cross-polarization magic angle spinning (CP-MAS) ^{13}C NMR spectroscopy on dried samples obtained from extruded (50 nm) and irradiated dispersions of **2** as well as solid samples of the protected and non-amphiphilic hexa(ethynylene) **1**, recorded under exactly identical acquisition and processing parameters. *B,D)* solution-phase, high-resolution ^{13}C NMR spectra of non-irradiated **2** and **1** (400 MHz, CD_2Cl_2 or d_6-DMSO). For the detailed assignment of carbon resonances, see Supplementary Figure S2. Notably, the signal intensity in (*A*) in the region of δ = 60–80 ppm that is a superposition of the 9 internal acetylene carbons (C11–C19), the carbohydrate carbons C2–C6, and the CH_2O carbon C7 of the propyl spacer significantly decreased, as compared to (*C*) . The irradiated sample (*A*) exhibited 6 distinct resonances in this region that can be tentatively assigned to C2–C7. Accordingly, the internal acetylene groups have apparently been consumed to a large extent. The fact that the position of the large resonance at about 75 ppm (which disappears in the process of carbonization) does not exactly match the positions of the acetylene carbons in solution can be attributed to the substantially different chemical environments in the bulk and in dilute DMSO solution; close packing of the oligo(ethynylene) segments in the bulk should result in π–π stacking and cause the observed downfield shift of the acetylene carbon resonances. The signal intensity in the region δ = 80–90 ppm that can be assigned to 3 terminal acetylene carbons (C10, C20, C21) has only slightly decreased, indicating that the associated triple bonds (in particular, those at the TIPS group; C20, C21) have reacted react more sluggishly. The significant increase in signal intensity at δ = 120–160 ppm can be attributed to the formation of sp^2 hybridized olefin or aromatic carbons, since no other carbons typically appear in this region. Finally, the observed distinct resonances of C1–C7 in the carbonized material proves that the carbohydrate groups remained structurally intact. For detailed experimental procedures on sample preparation, spectrum acquisition, and data processing for the solid state NMR spectra, see Experimental Part (Section 2 of the Supplementary Online Material).

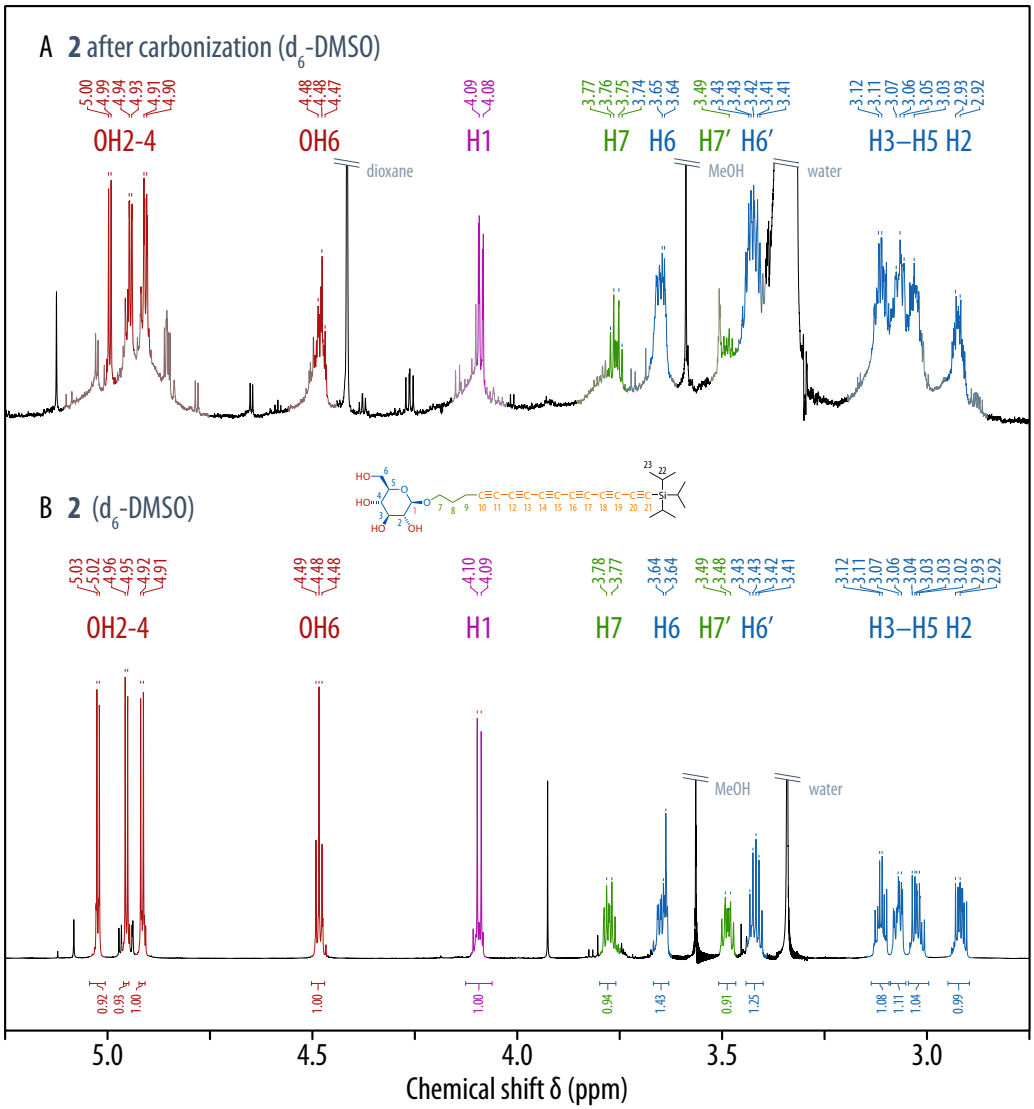

Figure S12. *A)* High-resolution solution-phase NMR spectrum (800 MHz, d_6-DMSO) of a sample of carbonized **2**, obtained by extrusion of an aqueous dispersion of **2** through a polycarbonate membrane with a pore size of 100 nm, followed by UV irradiation for 24 h at 1°C, drying of the dispersion, and redissolution in d_6-DMSO. *B)* High-resolution solution-phase NMR spectrum (800 MHz, d_6-DMSO) of pure **2**. The comparison of the two spectra allows to conclude that the carbohydrate groups are still intact in the carbonized nanocapsules. All ^{1}H resonances of the 4 carbohydrate OH groups (OH2-4 and OH6; red), the anomeric proton (H1, purple), the 5 remaining carbohydrate protons (H2–H6/H6', blue), as well as the CH_2O group of the propyl spacer (H7/H7', green) are clearly visible and can be assigned in the carbonized sample. All resonances have experienced peak duplication and further splitting, and each of the peaks emerges from broader resonances in the respective regions (shaded colors). All of this indicates that, after carbonization, various carbohydrate groups coexist in slightly different chemical environments. However, the fact that all peaks are still sharp and their principal shape has remained essentially unaffected shows that the carbohydrate head groups, even though they are attached to the highly cross-linked and rigid carbon scaffold, remain mobile (on the NMR time scale) and accessible to the polar medium. For detailed experimental procedures as well as the complete analytical data of **2**, see Experimental Part and the NMR Spectra Appendix (Sections 2 and 3 of the Supplementary Online Material).

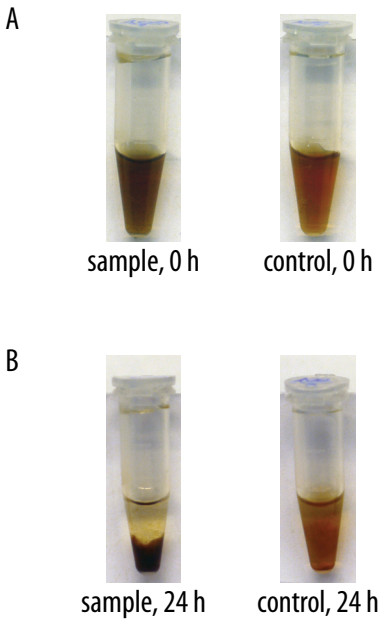

Figure S13. *A,B)* Representative examples of Concanavalin A essays applied to aqueous dispersions of carbon nanocapsules (and control samples). The samples were prepared by extrusion of aqueous dispersions of **2** using polycarbonate membranes with 50 nm pore size and UV irradiation for 24 h at 1°C. After the addition of Concanavalin A Texas Red® conjugate and the cofactors Ca^{2+} and Mn^{2+}, precipitation was observed after incubation of the sample for 24 h (*B*, left). In the case of control samples without Concanavalin A (but in the presence of all salts), no precipitation was observed. However, the dispersions became slightly cloudy, which was tentatively attributed to aggregation of the carbohydrate-covered nanocapsules due to the presence of the divalent cations.

2. Experimental Part

2.1 Instrumentation

UV/Vis spectroscopy was carried out on a Jasco V-670 (Gotha, Germany). Raman spectra of bulk samples and solutions were performed on a Jasco FT/IR 6300 spectrometer with an RFT-6000 Raman accessory using a 1064 nm laser. Raman spectroscopy on dried dispersions was performed on a custom-built micro-Raman setup using a Trivista 550 triple spectrometer. High-resolution ^{1}H and ^{13}C NMR spectroscopy for the molecular characterization of compounds **1–6** was carried out on a Bruker Avance 400 spectrometer operating at a frequency of 400.19 MHz for ^{1}H and 100.63 MHz for ^{13}C nuclei. High-resolution ^{1}H NMR spectroscopy of solutions of **1**, as well as solutions and dispersions of **2** before and after carbonization was performed on a Bruker Avance II 800 spectrometer operating at a frequency of 800.13 MHz for ^{1}H nuclei. Solid-state cross-polarization magic angle spinning (CP-MAS) ^{13}C NMR spectra of solid samples were acquired on a Bruker Avance 700 Spectrometer at ETH Zürich. High resolution mass spectra were recorded as service measurements at the Department of Chemistry and Applied Biosciences at ETH Zürich on a Bruker Daltonics maXis ESI spectrometer. X-ray Photoelectron Spectroscopy (XPS) was performed in the *Surface Analysis Facility* of the *Interdisciplinary Centre for Electron Microscopy* at EPFL on an Axis Ultra instrument (Kratos Analytical, Manchester, UK). SAXS measurements were performed using a Rigaku microfocused X-ray source. DLS measurements were performed using a 3D cross-correlation light scattering instrument from LS Instruments (Fribourg, Switzerland)

2.2 Materials and Methods

Preparation of Aqueous Dispersions and Vesicle Extrusion. Aqueous dispersions of **2** with different concentrations were prepared by injecting organic stock solutions of **2** (200 μL, 10 mg/mL in 1,4-dioxane/methanol 4:1) into MilliQ water (800 μL). The final dispersions exhibited concentrations of 2 mg/mL of **2** for cryo-TEM experiments and 3 mg/mL of **2** for SAXS measurements. The dispersions were vortexed four times every 10 min for 30 sec each. In order to convert the multi-lamellar vesicles into unilamellar vesicles with a controlled average diameter, the dispersions were extruded through polycarbonate membranes with the desired pore size (50, and 100 nm) using a miniextruder (Avanti Polar Lipids, Alabaster, USA).

Carbonization by UV Irradiation. The aqueous dispersions of **2** were placed into a double-mantle Schlenk tube, thermostated to 1°C, and exposed to UV irradiation for 24 h at this temperature, using a 250 W Ga-doped medium-pressure Hg light source (UV Light Technologies, Birmingham, UK) placed at a distance of 50 cm away from the Schlenk tube. Samples for UV spectroscopy were taken after 0.5, 1, 2, 4, 6, 9, 12, and 24 h.

Cryogenic Transmission Electron Microscopy (cryo-TEM). Samples for cryo-TEM imaging were prepared by the 'plunge freezing' method. For this purpose, a TEM grid (holey or lacey carbon) was fixed between tweezers, and 5 μL of the sample dispersion were placed onto the grid. The tweezers were subsequently mounted into a 'plunge freezing' apparatus and, after blotting, the grid was immediately dropped into a container filled with liquid ethane that was surrounded by liquid nitrogen. A Philips CM12 EM (Philips, Eindhoven, Netherlands) electron microscope operating at 100 keV was used to image the samples. The operation temperature was –180°C, and a cryo-specimen holder Gatan 626 (Warrendale, PA, USA) was used. Digital micrographs were recorded with a Gatan MultiScan CCD-camera.

Transmission Electron Microscopy (TEM). TEM imaging was performed on samples negatively stained with uranyl acetate. For this purpose, the dispersions used for cryo-experiments were 100–150fold diluted. Then, 5 μL of the sample dispersion were placed onto a carbon-coated copper grid (300 μm mesh) and incubated for 3 min. Afterwards, the grids were washed with MilliQ water. For the negative staining, 5 μL of aqueous uranyl acetate solution (2% *w/v*) were placed onto the grid for 30 s, and the excess solution was then removed with a filter paper. The samples were imaged with a Philips CM12 EM (Philips, Eindhoven, Netherlands) electron microscope operating at 100 keV.

X-Ray Photoelectron Spectroscopy (XPS). Sample solutions for XPS experiments were placed onto a SiO_2 surface and dried over night. XPS data were collected using an Axis Ultra instrument (Kratos analytical, Manchester, UK) under ultra-high vacuum condition ($<10^{-8}$ Torr) and a monochromatic Al Kα X-ray source (1486.6 eV), in the *Surface Analysis Facility of the Interdisciplinary Centre for Electron Microscopy* at EPFL. The source power was maintained at 150 W and the emitted photoelectrons were sampled from a 750 μm × 300 μm area. The analyzer pass energy was 80 eV for survey spectra and 40 eV for high-resolution spectra. Both curve fitting of the spectra and quantification were performed with the CasaXPS software, using relative sensitivity factors given by Kratos and on the basis of reference spectra for Cellulose and Cellulose triacetate found in *The XPS of Polymers Database* (G. Beamson and D. Briggs, eds., Surface Spectra Ltd.).

Dynamic Light Scattering (DLS). DLS measurements on dispersions of **2** before and after carbonization were performed using a 3D cross-correlation light scattering instrument from LS Instruments (Fribourg, Switzerland) equipped with a He-Ne laser emitting a polarized light beam of a wavelength of 632.8 nm. Samples were filled into glass tubes with a diameter of 10 mm. The scattered intensity fluctuations were collected at a fixed angle of 90° by averaging 3 runs of 600 sec each and converted into the electric field time correlation functions. In order to determine the exact viscosity of the dioxane/MeOH/MilliQ mixture needed for particle sizing of the vesicles, a calibration test was run first in identical solvent conditions using standard 610 nm polystyrene nanoparticles (Bangs Laboratories),

and the exact viscosity was extracted via the decay rate of the electric field time correlation function of the standard nanoparticles. The time correlation function (TCF) of the electric field, was then analyzed by the CONTIN method to yield particle size distribution.

Small-Angle X-Ray Scattering (SAXS). SAXS measurements on dispersions of **2** after carbonization were performed using a Rigaku microfocused X-ray source of wavelength $\lambda = 1.54$ Å operating at 45 kV and 88 mA. The scattered X-ray signal was collected on a gas-filled 2D detector. The scattering vector q was calibrated using silver behenate. Samples were filled into a capillary with a diameter of 1 mm. Data were collected and azimuthally averaged to yield 1D intensity versus scattering vector q. The fitting model was implemented using the software modules supplied by the National Institute of Science and technology (NIST), Washington D.C., USA [7].)

Micro-Raman Spectroscopy. Multiwavelength Raman spectroscopy was performed at ambient conditions using a back-scattering geometry for the 457.9 nm, 488.0 nm, 514.5 nm and 530.9 nm excitation lines of an Ar^+Kr^+ ion laser. The laser was focused to a diffraction-limited spot using a microscope objective with numerical aperture NA = 0.75. The power of the incident light was 500 μW. The scattered light was collected by a triple spectrometer coupled with a multichannel CCD detector. Room temperature photoluminescence experiments were carried out using the 488.0 nm laser line for excitation at a laser power of 100 μW. The incident light was focused on the surface of the liquid sample with a long working distance objective (WD = 35 mm, NA=0.13). The luminescence was detected by a grating spectrometer equipped with a CCD device.

Solid State Cross Polarization Magic Angle Spinning (CP-MAS) ^{13}C NMR Spectroscopy. ^{13}C NMR spectra of solid samples were acquired using identical experimental parameters for all samples on a Bruker Avance 700 Spectrometer at a magnetic field of 16.4 T (700 MHz ^1H frequency). The samples were spun at the magic angle with a rate of 24.00 kHz, using ZrO rotors with an outer diameter of 2.5 mm and a double resonance probehead tuned to the frequencies of ^1H (700.13 MHz) and ^{13}C nuclei (176.06 MHz). A Cross Polarization (CP) pulse sequence with TPPM ^1H heteronuclear decoupling during acquisition was used. After an initial $\pi/2$ pulse on ^1H with a duration of 2.5 μs, a CP period was used with a duration of 4 ms. This pulse employed a tangential variation of the ^1H rf field around the (experimentally) optimized Hartmann-Hahn condition with a central amplitude of 100 kHz on ^1H and 76 kHz on ^{13}C. The TPPM decoupling had an amplitude of 100 kHz and a pulse of 5.3 μs. The acquisition had a duration of 29 ms and a length of 4096 points for a sweepwidth of 400 ppm. The recycle delay was set to 1.0 s, and a total of 81920 fid's were added. The spectra were zero-filled to 8192 complex points and apodized with a 128 Hz exponential broadening function prior to the Fourier transformation. An identical polynomial baseline correction was used on all spectra.

Concanavalin A Essay. 10 μL of an aqueous solution of Concanavalin A Texas Red® conjugate (Invitrogen, Carlsbad, USA; 10 mg/mL in 1 M NaCl) were added to an aqueous solution of carbon capsules (200 μL, 2 mg/mL; aqueous dispersions of **2** after extrusion using a polycarbonate membrane with 50 nm or 100 nm pore size and UV irradiation for 24 h at 1°C) containing $CaCl_2$ (1 mmol/L) and $MnCl_2$ (1 mmol/L). For the control samples, 10 μL of an aqueous solution of NaCl (1 M) were added to an aqueous dispersion of carbon capsules (200 μL, 2 mg/mL, prepared as described before) containing $CaCl_2$ (1 mmol/L) and $MnCl_2$ (1 mmol/L). All samples were vortexed and incubated for 24h at room temperature.

*2.3 Synthetic Procedures and Analytical Data for Compounds **1–6***

General Synthesis Procedures. Unless otherwise noted, all reactions were carried out in dried Schlenk glassware in an inert argon atmosphere. Solvents were purchased as reagent grade and distilled prior to use. For reactions, DCM, acetonitrile, toluene, and THF were purchased as HPLC grade and purified with a solvent purification system from Innovative Technologies. All reagents were commercially obtained and used without further purification. MeOH (99.8% Extra Dry over Molecular Sieves), MeLi · LiBr (2.2 M in Et_2O), $ZnCl_2$ (0.7 M in THF), $AgNO_3$, and NBS were purchased from Acros Organics. AgF and Amberlite IR-120 (H^+) were purchased from abcr GmbH & Co. KG, Germany, NaOMe was purchased from Fluka, and $PdCl_2$(dppf) · DCM was purchased from Boron Molecular, USA. TLC analyses were performed on TLC plates from Merck (Silica gel 60 F_{254}). UV-light (254 nm) or anisaldehyde staining was used for detection. Column chromatography was conducted on Geduran gel Si 60 from Merck (40-60 μm).

*4'-Pentynyl 2,3,4,6-tetra-O-acetyl-β-D-glucopyranoside **3***.
β-D-Glucose pentaacetate (47.25 g, 121.05 mmol) and 4-pentyn-1-ol (15.71 g, 186.76 mmol) were dissolved in DCM (600 mL). The mixture was cooled to 0°C, and boron trifluoride etherate (35.4 g, 249.44 mmol) was added. The cooling bath was removed, and the reaction was stirred for 7 h. The mixture was washed three times with saturated aqueous $NaHCO_3$ solution and once with saturated aqueous NaCl solution. The organic phase was dried over $MgSO_4$, and column chromatography (silica gel, heptane: EtOAc) yielded **3** (23.55 g, 47%) as a colorless syrup which solidified after two days. ^{1}H NMR (400 MHz, CD_2Cl_2): δ = 5.19 (dd, *J* = 9.6 Hz, 1H), 5.03 (dd, *J* = 9.9 Hz, 1H), 4.91 (dd, *J* = 8.0 Hz, 9.7 Hz, 1H), 4.51 (d, *J* = 8.0 Hz, 1H), 4.24 (dd, *J* = 4.8 Hz, 12.3 Hz, 1H), 4.09 (dd, *J* = 2.5 Hz, 12.3 Hz, 1H), 3.92 (dt, *J* = 5.7 Hz, 9.8 Hz, 1H), 3.71 (ddd, *J* = 2.5 Hz, 4.8 Hz, 10.0 Hz, 1H), 3.62 (ddd, *J* = 5.4 Hz, 7.7 Hz, 9.8 Hz, 1H), 2.23 (dt, *J* = 2.7 Hz, 6.7 Hz, 7.4 Hz, 2H), 2.05 (s, 3H), 2.02 (s, 3H), 1.99 (s, 3H), 1.98 (t, *J* = 2.7 Hz, 1H), 1.96 (s, 3H), 1.83-1.70 (m, 2H). ^{13}C NMR (101 MHz, CD_2Cl_2) δ

= 170.9, 170.5, 169.9, 169.8, 101.5, 83.9, 73.2, 72.3, 71.8, 69.1, 69.0, 69.0, 62.5, 28.9, 21.0, 21.0, 21.0, 20.9, 15.3. HRMS (ESI): calcd $C_{19}H_{30}NO_{10}$: ($[M+NH_4]^+$) 432.1864; found 432.1870, R_f: 0.39 (EtOAc/*n*-heptane 1:1).

*5'-Bromopent-4'-ynyl 2,3,4,6-tetra-O-acetyl-β-D-glucopyranoside **4**.*

Pent-4'-ynyl 2,3,4,6-tetra-*O*-acetyl-β-D-glucopyranoside **3** (12.49 g, 30.15 mmol) was dissolved in MeCN (250 mL), and the flask was wrapped with aluminum foil. *N*-Bromosuccinimide (5.15 g, 31.60 mmol) and $AgNO_3$ (2.55 g, 15.01 mmol) were added, and the mixture was stirred for 15 h. The reaction was quenched by the addition of a concentrated aqueous KCl solution (1.33 g, 17.77 mmol KCl). The mixture was filtered through a paper filter and precipitated into deionized water (3 L). The mixture was stirred for 2 days, and the precipitate was filtered and redissolved with acetone. The solution was concentrated, DCM was added, and the solution was washed once with water and once with saturated aqueous NaCl solution. The organic phase was dried over $MgSO_4$ and evaporated *in vacuo* to yield 5'-bromopent-4'-ynyl 2,3,4,6-tetra-*O*-acetyl-β-D-glucopyranoside **4** (13.77 g, 93%) as a colorless solid. ^{1}H NMR (400 MHz, CD_2Cl_2): δ = 5.19 (dd, *J* = 9.6 Hz, 1H), 5.03 (dd, *J* = 9.7 Hz, 1H), 4.91 (dd, *J* = 8.0 Hz, 9.7 Hz, 1H), 4.50 (d, *J* = 8.0 Hz, 1H), 4.24 (dd, *J* = 4.9 Hz, 12.3 Hz, 1H), 4.09 (dd, *J* = 2.5 Hz, 12.3 Hz, 1H), 3.90 (dt, *J* = 5.6 Hz, 9.9 Hz, 1H), 3.72 (ddd, *J* = 2.5 Hz, 4.8 Hz, 10.0 Hz, 1H), 3.59 (ddd, *J* = 5.4 Hz, 7.7 Hz, 9.8 Hz, 1H), 2.27 (t, *J* = 7.0 Hz, 2H), 2.05 (s, 3H), 2.02 (s, 3H), 1.99 (s, 3H), 1.97 (s, 3H), 1.83-1.68 (m, 2H). ^{13}C NMR (101 MHz, CD_2Cl_2) δ = 171.0, 170.5, 169.9, 169.8, 101.5, 79.9, 73.2, 72.3, 71.8, 69.0, 68.9, 62.5, 38.5, 28.7, 21.0, 21.0, 21.0, 21.0, 16.5. HRMS (ESI): calcd $C_{19}H_{25}O_{10}BrNa$: ($[M+Na]^+$) 515.0523; found 515.0530. R_f: 0.39 (EtOAc/*n*-heptane 1:1).

*9'-Trimethylsilylnona-4',6',8'-triynyl 2,3,4,6-tetra-O-acetyl-β-D-glucopyranoside **5**.*

MeLi · LiBr complex (18.5 mL, 2.2 M in Et_2O, 40.70 mmol) was added to 1,4-bis(trimethylsilyl)butadiyne (8.08 g, 41.56 mmol) in THF (65 mL) at 0 °C, and the resulting mixture was stirred for 30 minutes. Then $ZnCl_2$ (60 mL, 0.7 M in THF, 42.0 mmol) was added at 0 °C, and the resulting mixture was again stirred for 30 minutes. In another flask, 5'-bromopent- 4'-ynyl 2,3,4,6-tetra-*O*-acetyl-β-D-glucopyranoside **4** (10.00 g, 20.27 mmol), and $PdCl_2$(dppf) · DCM (1.66 g, 2.03 mmol) were mixed in toluene (300 mL). The two solutions were combined at 0 °C, and the flask was wrapped with aluminum foil. The mixture was stirred for 20h at 0 °C, before it was diluted with Et_2O, washed once with sat. NH_4Cl solution and once with sat. NaCl solution. The organic phase was dried over $MgSO_4$, and concentrated in vacuo. Column chromatography (silica gel; EtOAc/n-heptane 1:2) yielded **5** (8.37 g, 77%) as a light brown solid. ^{1}H NMR (400 MHz, CD_2Cl_2): δ = 5.19 (dd, *J* = 9.6 Hz, 1H), 5.03 (dd, *J* = 9.9 Hz, 1H), 4.90 (dd, *J* = 8.0 Hz, 9.7 Hz, 1H), 4.50 (d, *J* = 8.0 Hz, 1H), 4.24 (dd, *J* = 4.9 Hz, 12.3 Hz, 1H), 4.09 (dd, *J* = 2.5 Hz, 12.3 Hz, 2. 1H), 3.90 (dt, *J* = 5.5 Hz, 9.9 Hz, 1H), 3.72 (ddd, *J* = 2.5 Hz, 4.9 Hz, 10.0 Hz, 1H), 3.59 (ddd, *J* = 5.2 Hz, 7.8 Hz, 9.9 Hz, 1H), 2.38 (t, *J* = 7.0 Hz, 2H), 2.05 (s, 3H), 2.02 (s, 3H), 1.99 (s, 3H), 1.96 (s, 3H), 1.88-1.72 (m, 2H), 0.19 (s, 9H). ^{13}C NMR (101 MHz, CD_2Cl_2) δ = 170.9, 170.5, 169.9, 169.8, 101.5, 88.3, 86.5, 80.7, 73.2, 72.4, 71.7, 69.0, 68.7, 66.1, 62.5, 62.4, 60.4, 28.4, 21.0, 21.0, 21.0, 20.9, 16.4, -0.3. IR (ATR) ν 2960, 2939, 2898, 2206, 2163, 2072, 1745, 1378, 1365, 1240, 1206, 1165, 1068, 1035 (cm^{-1}). UV (MeCN) λ_{max} (log ε) 220 (5.02), 209 (5.06), 200 (4.89) nm. $[\alpha]_D$ 149.8 (c 0.21, MeCN). HRMS (ESI): calcd for $C_{26}H_{34}O_{10}SiNa$ ($[M+Na]^+$) 557.1813; found 557.1832. R_f: 0.40 (EtOAc/*n*-heptane 1:1).

*9'-Bromonon-4',6',8'-triynyl 2,3,4,6-tetra-O-acetyl-β-D-glucopyranoside **6**.*

9'-Trimethylsilylnona-4',6',8'-triynyl 2,3,4,6-tetra-*O*-acetyl-β-D-glucopyranoside **5** (3.50 g, 6.55 mmol) was dissolved in dry MeCN (80 mL) and the flask was wrapped with aluminum foil. *N*-Bromosuccinimide (1.23 g, 6.87 mmol) and $AgNO_3$ (872 mg, 6.87 mmol) were added and the resulting mixture was stirred for 3 hours. The mixture was precipitated into DI water (1 L), the precipitate was filtered to yield **6** (2.86 g, 81%) as a yellow solid. ^{1}H NMR (400 MHz, CD_2Cl_2): δ = 5.19 (dd, *J* = 9.6 Hz, 1H), 5.03 (dd, *J* = 9.7 Hz, 1H), 4.90 (dd, *J* = 8.0 Hz, 9.7 Hz, 1H), 4.50 (d, *J* = 8.0 Hz, 1H), 4.24 (dd, *J* = 4.9 Hz, 12.3 Hz, 1H), 4.09 (dd, *J* = 2.4 Hz, 12.3 Hz, 1H), 3.90 (dt, *J* = 5.5 Hz, 9.9 Hz, 1H), 3.72 (ddd, *J* = 2.5 Hz, 4.8 Hz, 10.0 Hz, 1H), 3.59 (ddd, *J* = 5.2 Hz, 7.8 Hz, 9.9 Hz, 1H), 2.37 (t, *J* = 7.0 Hz, 2H), 2.05 (s, 3H), 2.02 (s, 3H), 1.99 (s, 3H), 1.96 (s, 3H), 1.89-1.71 (m, 2H). ^{13}C NMR (101 MHz, CD_2Cl_2) δ = 170.9, 170.5, 169.9, 169.8, 101.4, 79.7, 73.1, 72.4, 71.7, 68.9, 68.7 66.2, 65.9, 62.4, 60.6, 60.1, 40.4, 28.4, 21.0, 21.0, 21.0, 20.9, 16.3. IR (ATR) ν 2958, 2931, 2878, 2218, 2186, 1738, 1426, 1373, 1232, 1206, 1161, 1092, 1066, 1052, 1035 (cm^{-1}). UV (MeCN) λ_{max} (log

ε) 212 (4.97) nm. $[\alpha]_D$ 127.75 (c 0.24, MeCN). HRMS (ESI): calcd for $C_{23}H_{25}BrO_{10}Na$ ($[M+Na]^+$) 563.0523; found 563.0526. R_f: 0.35 (EtOAc/*n*-heptane 1:1).

15'-Triisopropylsilylpentadeca-4',6',8',10',12',14'-hexynyl 2,3,4,6-tetra-O-acetyl-β-D-glucopyranoside ***1***. MeLi · LiBr complex (0.84 mL, 2.2 M in Et_2O, 1.85 mmol) was added to 1-triisopropylsilyl-6-trimethysilylbuta-1,3,5-triyne (577 mg, 1.91 mmol), in THF (4 mL) at 0 °C, and the resulting mixture was stirred for 30 minutes. Then, $ZnCl_2$ (2.70 mL, 0.7 M in THF, 1.89 mmol) was added at 0 °C, and the resulting mixture was again stirred for 30 minutes. In another flask, 9'-bromonon-4',6',8'-triynyl 2,3,4,6-tetra-*O*-acetyl-β-D-glucopyranoside **6** (0.50 g, 0.92 mmol), and $PdCl_2$(dppf) · DCM (115 mg, 0.14 mmol) were mixed in toluene (15 mL). The two solutions were combined at 0 °C, and the flask was wrapped with aluminum foil. The mixture was stirred for 78 h at 0 °C, before it was diluted with Et_2O, washed once with sat. NH_4Cl solution and once with sat. NaCl solution. The organic phase was dried over $MgSO_4$, and concentrated in vacuo. Column chromatography (silica gel; EtOAc/*n*-heptane 1:2) yielded **1** (0.35 g, 55%) as a brown syrup. ^{1}H NMR (400 MHz, CD_2Cl_2): δ = 5.19 (dd, *J* = 9.6 Hz, 1H), 5.02 (dd, *J* = 9.7 Hz, 1H), 4.90 (dd, *J* = 8.1 Hz, 9.6 Hz, 1H), 4.51 (d, *J* = 8.0 Hz, 1H), 4.24 (dd, *J* = 4.8 Hz, 12.3 Hz, 1H), 4.09 (dd, *J* = 2.3 Hz, 12.3 Hz, 1H), 3.96–3.82 (m, 1H) 3.72 (ddd, *J* = 2.3 Hz, 4.6 Hz, 9.9 Hz, 1H), 3.59 (ddd, *J* = 5.2 Hz, 7.7 Hz, 9.7 Hz, 1H), 2.42 (t, *J* = 6.9 Hz, 2H), 2.04 (s, 3H), 2.01 (s, 3H), 1.99 (s, 3H), 1.96 (s, 3H), 1.89-1.73 (m, 2H), 1.17-1.00 (m, 21H). ^{13}C NMR (101 MHz, CD_2Cl_2) δ = 170.9, 170.5, 169.9, 169.8, 101.4, 89.7, 87.8, 82.1, 73.2, 72.4, 71.7, 68.9, 68.6, 66.2, 63.5, 63.3, 62.9, 62.8, 62.5, 62.4, 61.7, 61.5, 60.6, 28.4, 21.0, 21.0, 21.0, 20.9, 18.8, 16.6, 11.8. IR (ATR) ν 2943, 2866, 2208, 2165, 2069, 2037, 1749, 1461, 1427, 1366, 1214, 1169, 1035 (cm^{-1}). UV (MeCN) λ_{max} (log ε) 296 (5.46), 280 (5.32), 266 (4.98), 252 (4.64) nm. $[\alpha]_D$ 150.92 (c 0.21, MeCN). HRMS (ESI): calcd for $C_{38}H_{50}NO_{10}Si$ ($[M+NH_4]^+$) 708.3198; found 708.3212. R_f: 0.45 (EtOAc/*n*-heptane 1:1).

*15'-Triisopropylsilylpentadeca-4',6',8',10',12',14'-hexynyl β-D-glucopyranoside **2**.*

15'-Triisopropylsilylpentadeca-4',6',8',10',12',14'-hexynyl 2,3,4,6-tetra-*O*-acetyl-β-D-glucopyranoside **1** (10.5 mg, 0.015 mmol) was dissolved in 1,4-dioxane (2 mL), and MeOH (0.4 mL) was added. NaOMe (1 mg, 0.017 mmol) was added, and the resulting mixture was stirred for 2 hours Then, Amberlite IR-120 (H^+) was added until the solution was neutralized, and the resulting mixture was stirred for 30 minutes. The solution was filtered from the Amberlite and transferred into a brown glass vial using a syringe with a fine needle. The crude compound was purified by column chromatography (silica gel; EtOAc/MeOH 4:1). Freeze-drying yielded **2** as a yellow oil that was immediately redissolved in dioxane/MeOH and stored in the refrigerator. ^{1}H NMR (400 MHz, DMSO) δ 5.01 (d, *J* = 4.8 Hz, 1H), 4.93 (d, *J* = 4.8 Hz, 1H), 4.89 (d, *J* = 5.0 Hz, 1H), 4.47 (dd, *J* = 5.9 Hz, 1H), 4.09 (d, *J* = 7.8 Hz, 1H), 3.78 (dt, *J* = 6.0 Hz, 10.2 Hz, 1H), 3.65 (ddd, *J* = 1.9 Hz, 5.6 Hz, 11.6 Hz, 1H), 3.54–3.37 (m, 2H), 3.15–2.98 (m, 3H), 2.92 (ddd, *J* = 4.8 Hz, 7.9 Hz, 8.9 Hz, 1H), 2.59 (t, *J* = 7.1 Hz, 2H), 1.83–1.71 (m, 2H), 1.09–1.01 (m, 21H). ^{13}C NMR (101 MHz, DMSO) δ = 102.8, 88.6, 87.9, 84.7, 76.8, 76.6, 73.4, 70.0, 66.9, 64.5, 63.7, 63.0, 62.3, 62.1, 61.7, 61.0, 60.9, 60.7, 59.3, 27.6, 18.3, 15.6, 10.6. HRMS (ESI): calcd for $C_{30}H_{38}NaO_6Si$ ($[M+Na]^+$) 545.2330; found 545.2333. R_f: 0.09 (EtOAc).

3. NMR Spectra of Compounds 1–6

^{1}H NMR spectrum (CD_2Cl_2, 400 MHz) of **3**

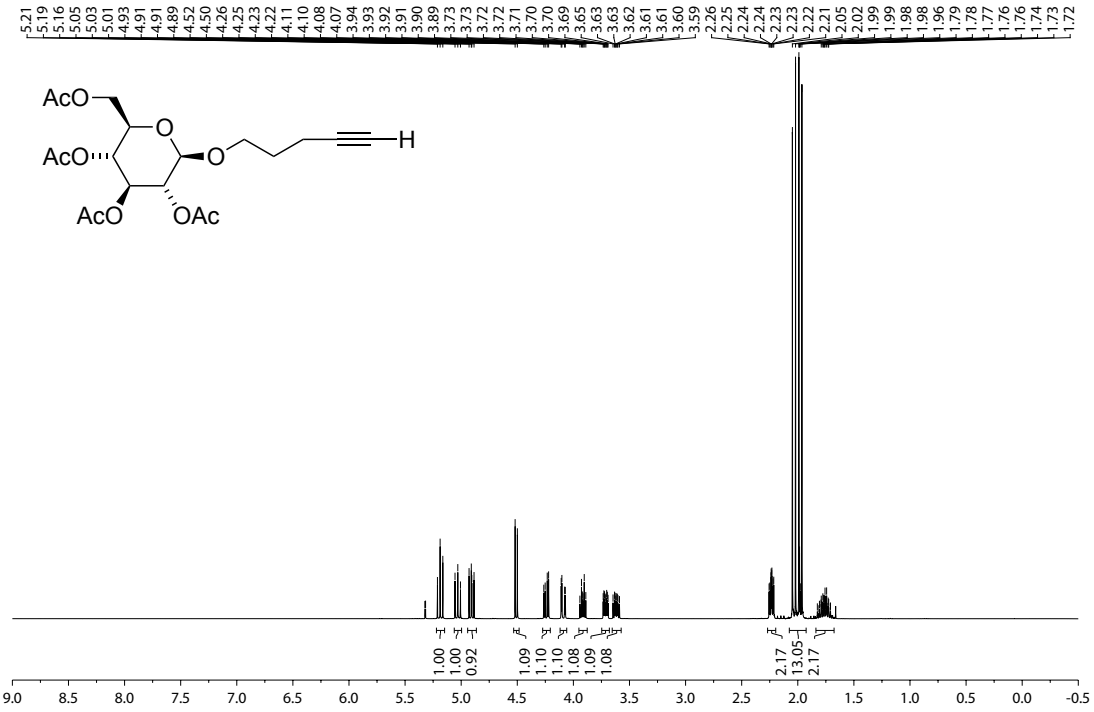

^{13}C NMR spectrum (CD_2Cl_2, 101 MHz) of **3**

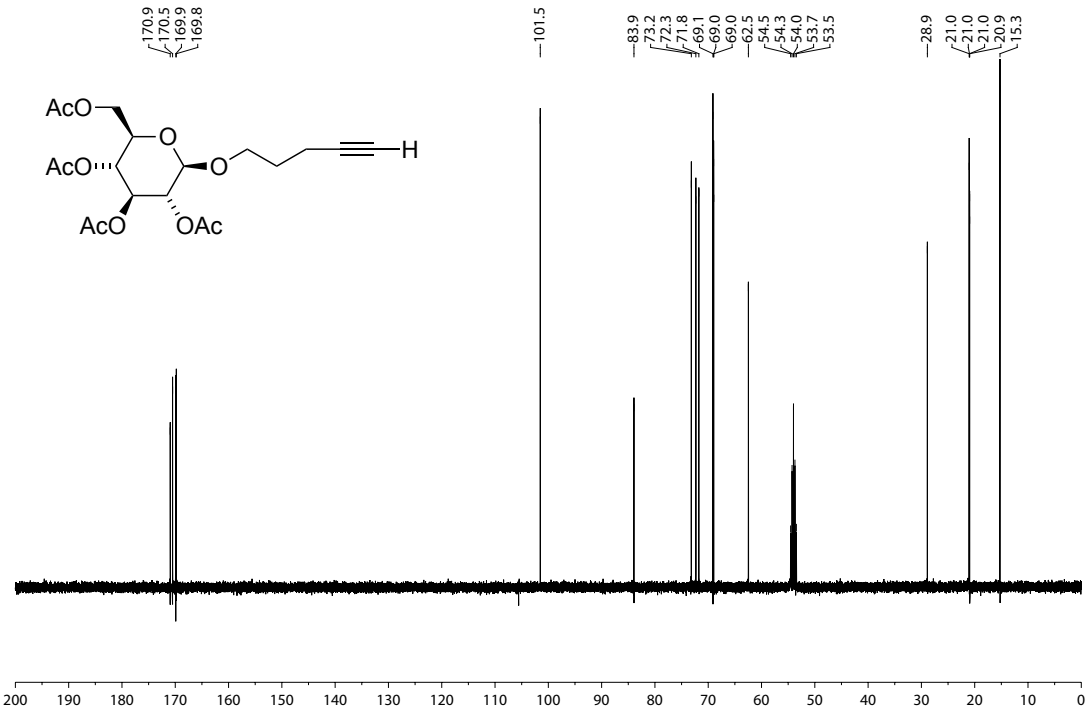

^{1}H NMR spectrum (CD_2Cl_2, 400 MHz) of **4**

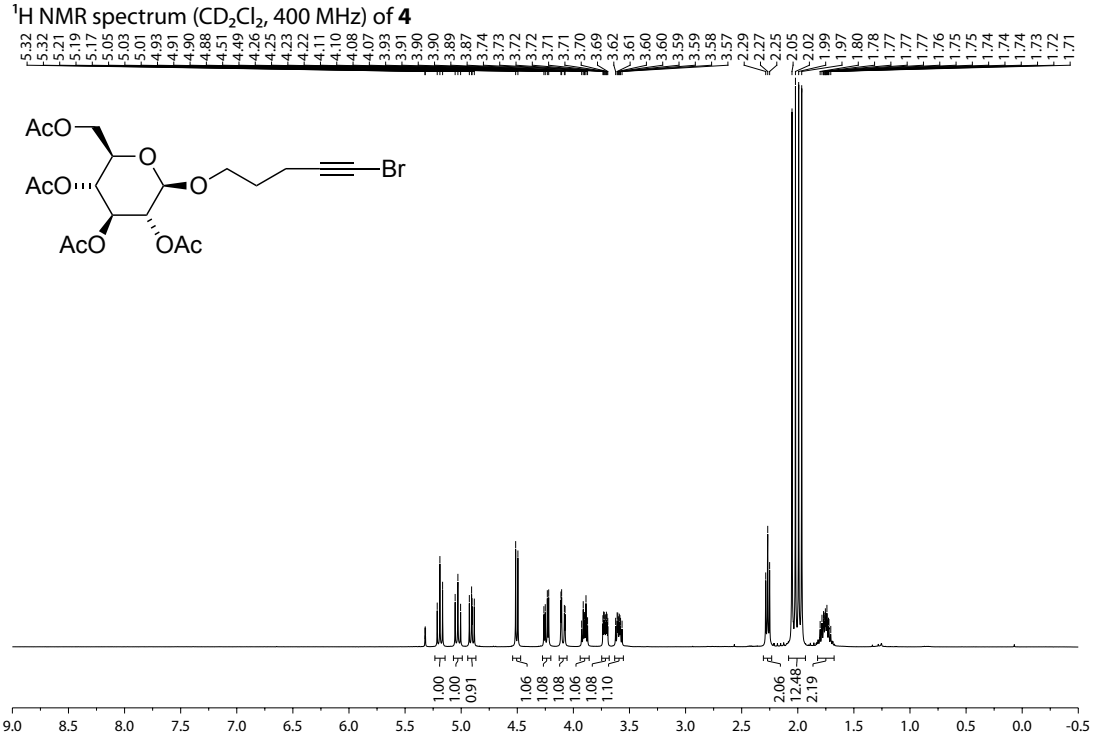

^{13}C NMR spectrum (CD_2Cl_2, 101 MHz) of **4**

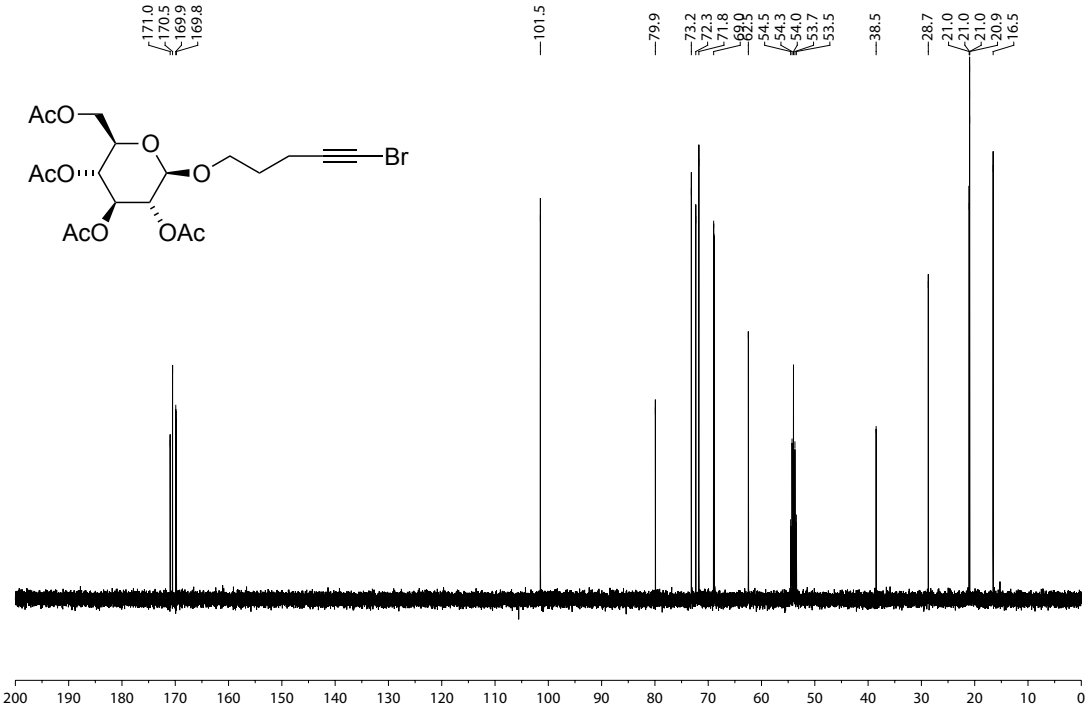

^{1}H NMR spectrum (CD_2Cl_2, 400 MHz) of **5**

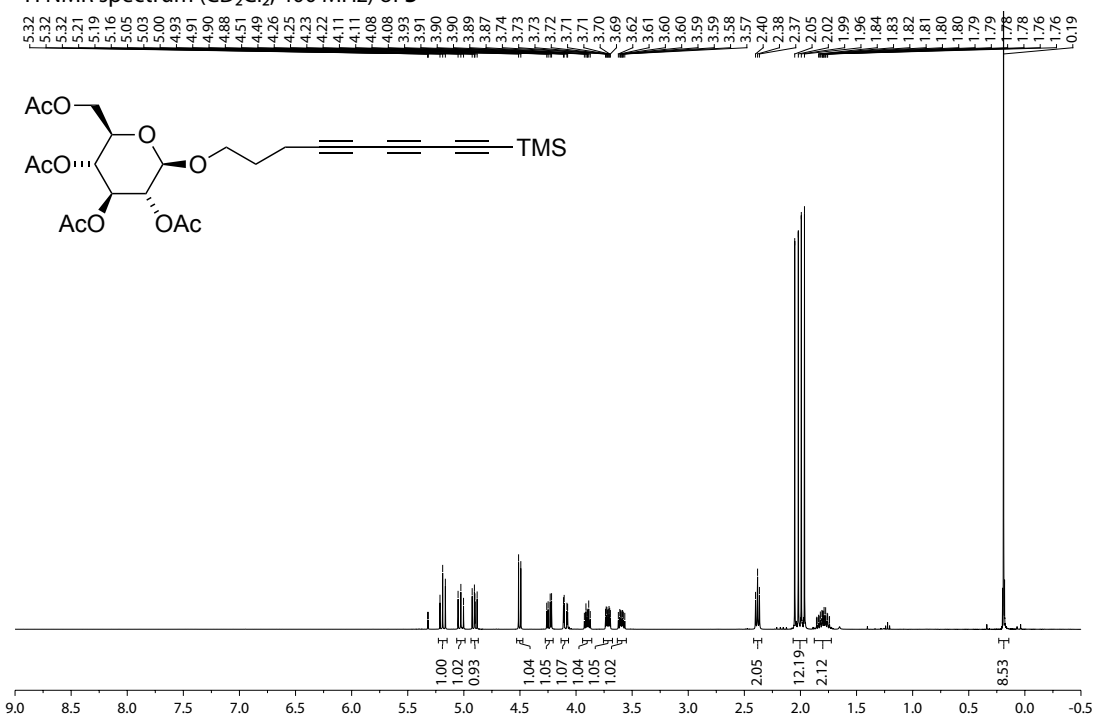

^{13}C NMR spectrum (CD_2Cl_2, 101 MHz) of **5**

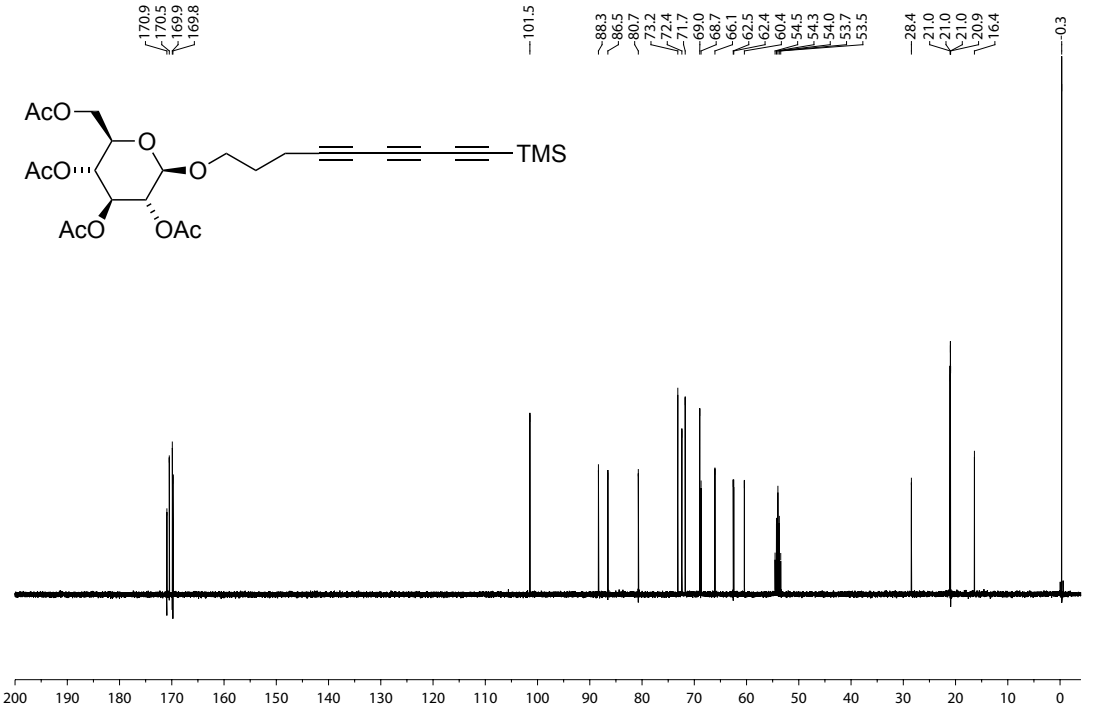

^{1}H NMR spectrum (CD_2Cl_2, 400 MHz) of **6**

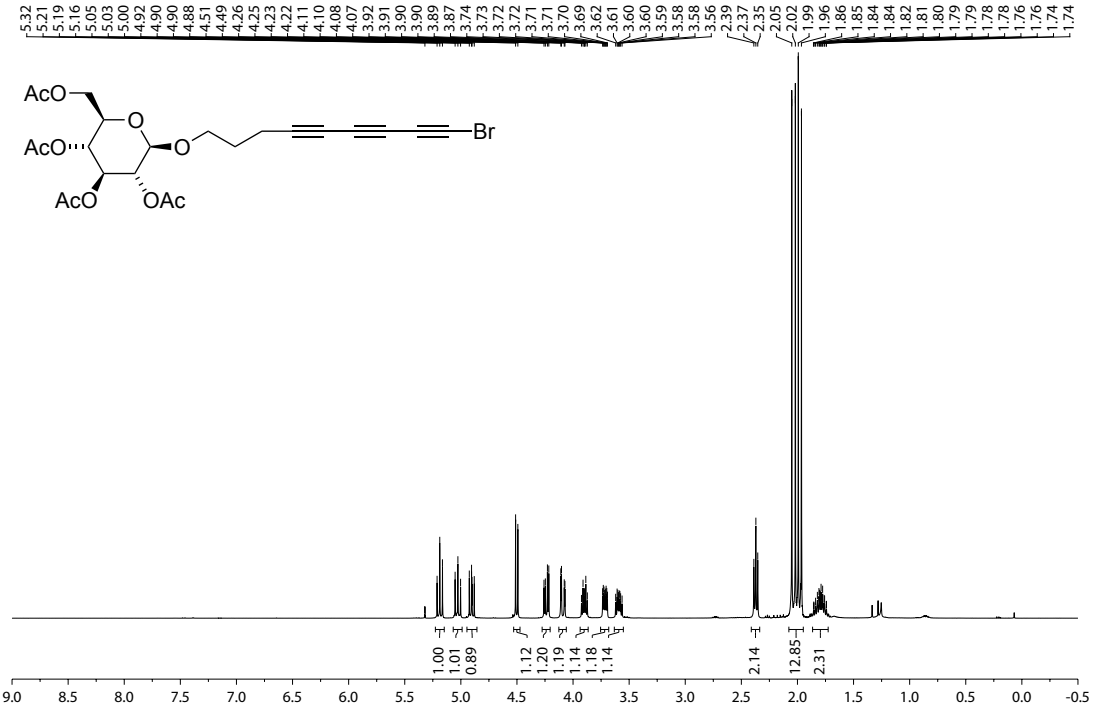

^{13}C NMR spectrum (CD_2Cl_2, 101 MHz) of **6**

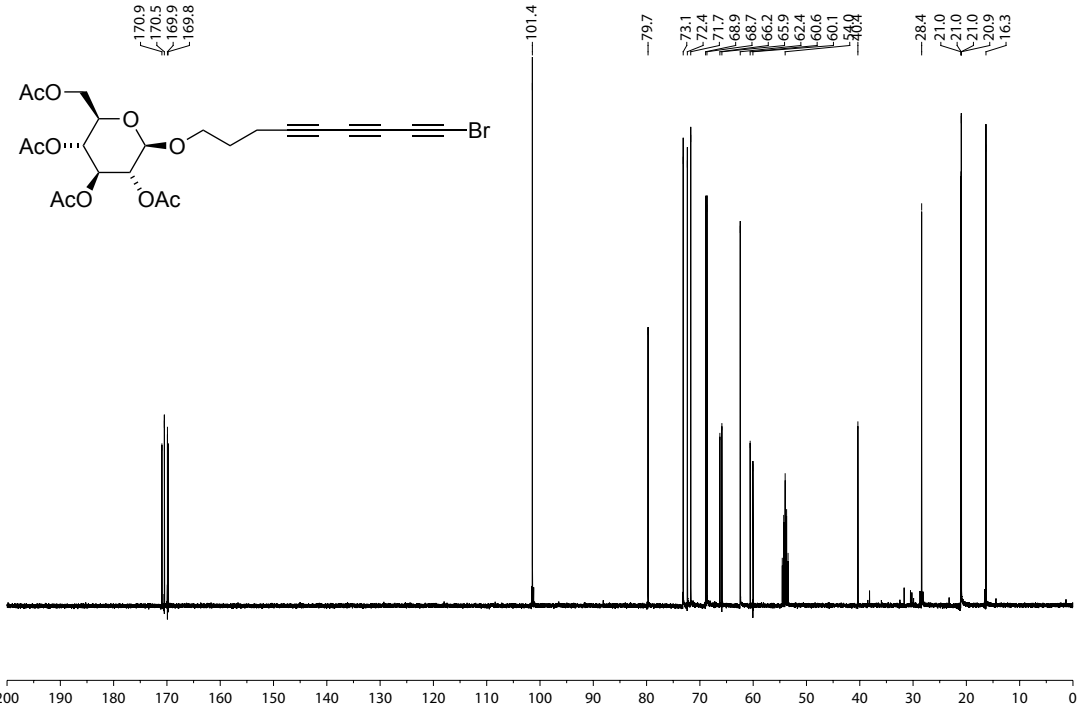

^{1}H NMR spectrum (CD_2Cl_2, 400 MHz) of **1**

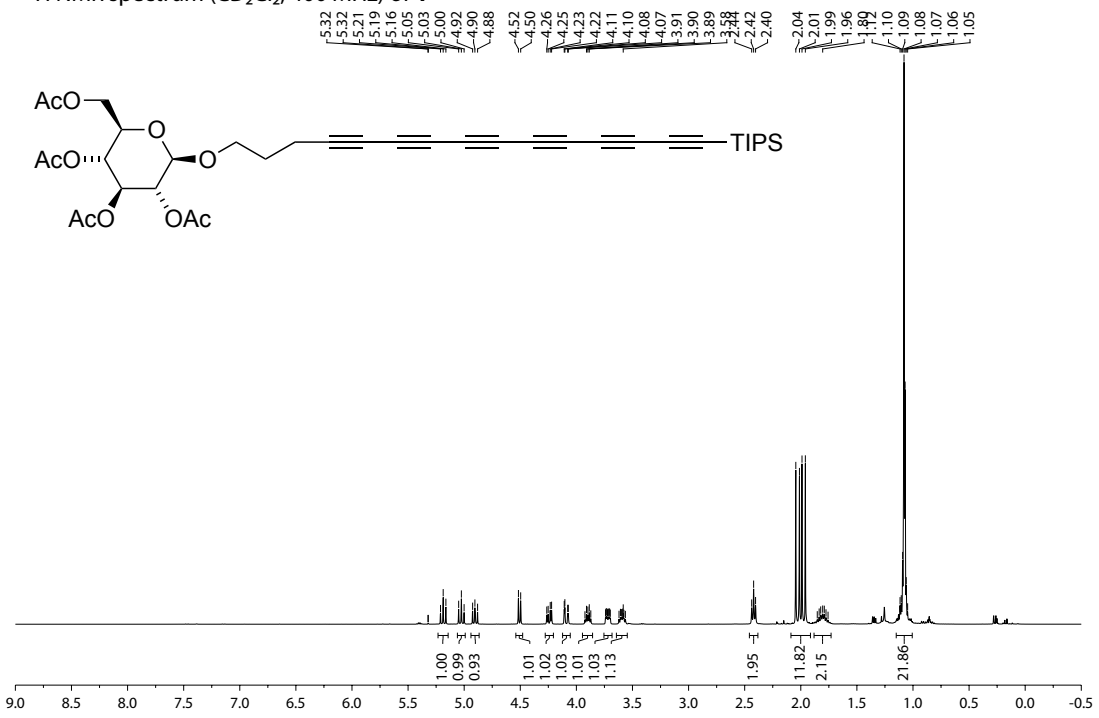

^{13}C NMR spectrum (CD_2Cl_2, 101 MHz) of **1**

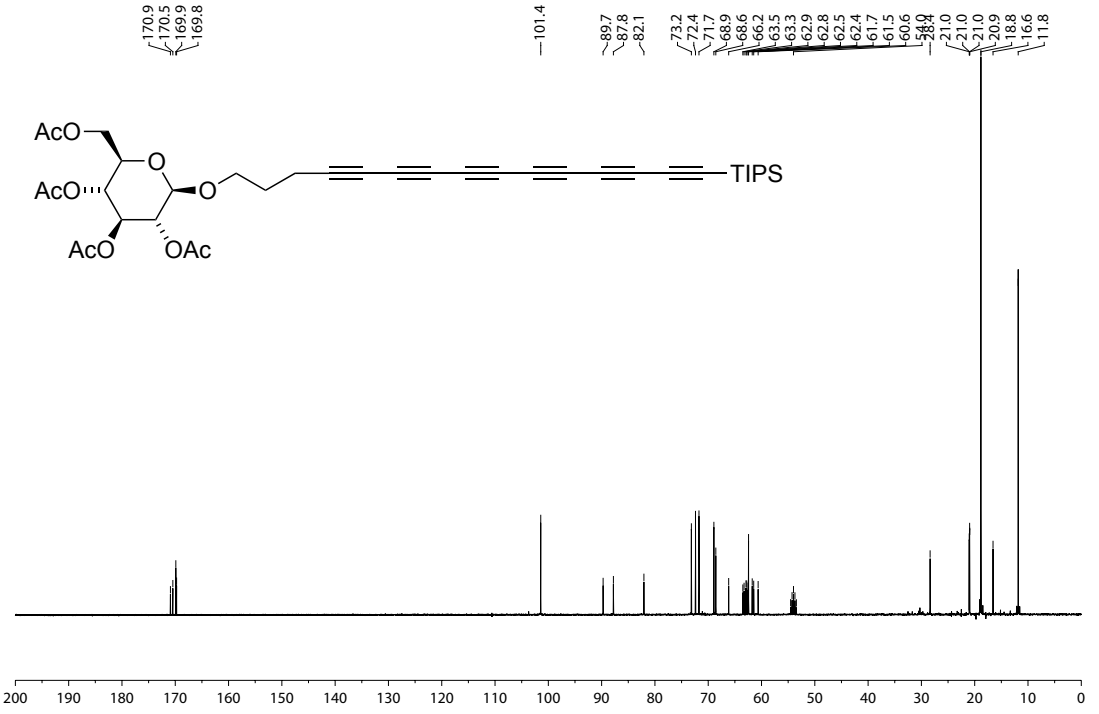

^{1}H NMR spectrum (DMSO-d_6, 400 MHz) of **2**

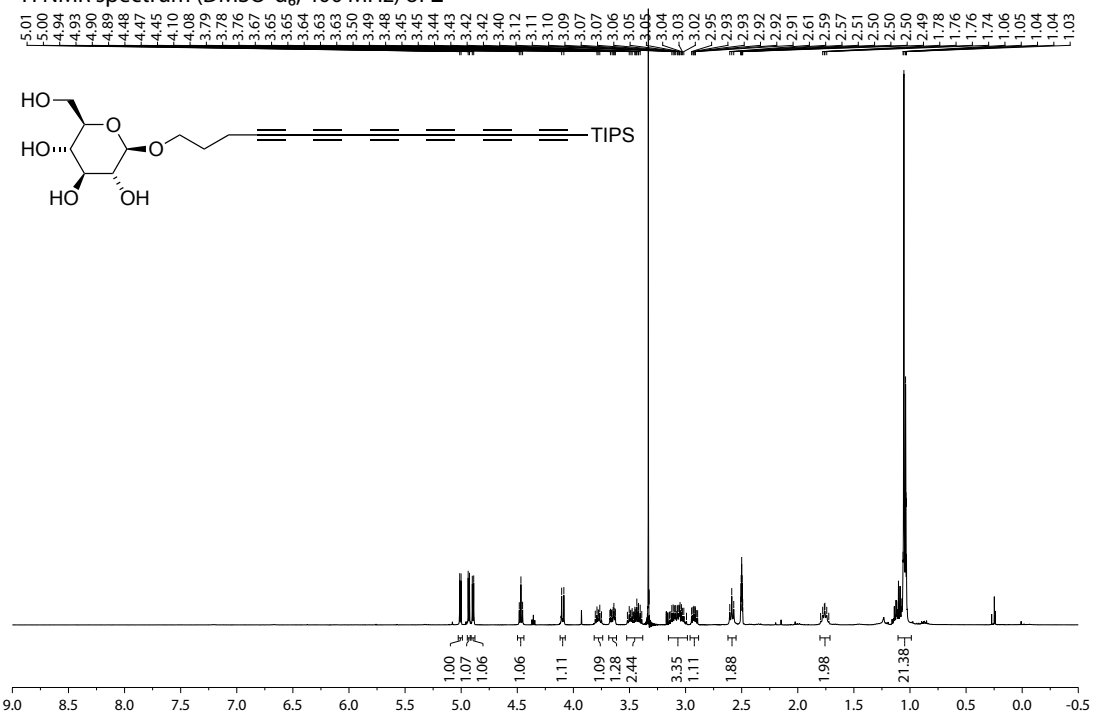

^{13}C NMR spectrum (DMSO-d_6, 101 MHz) of **2**

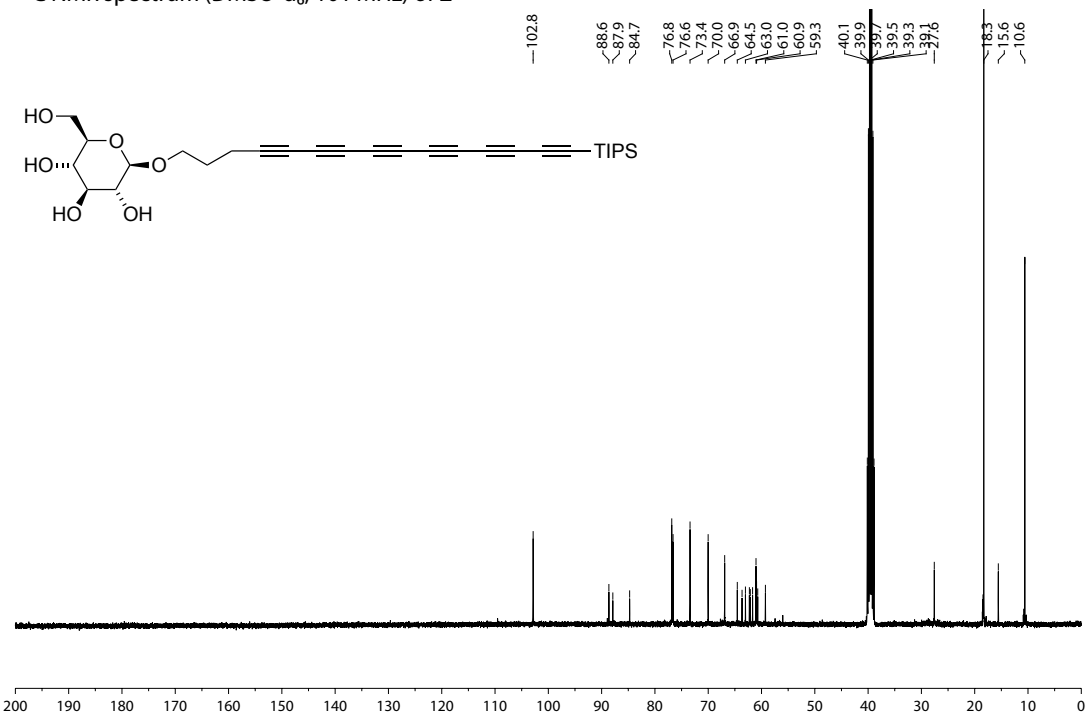

4. References

1 Hofmeister, H., Annen, K., Laurent, H. & Wiechert, R. New route to 17a-bromo- and 17a-iodoethynyl steroids. *Angew. Chem.* **96**, 720-721, (1984).

2 Kim, S., Kim, S., Lee, T., Ko, H. & Kim, D. A new, iterative strategy for the synthesis of unsymmetrical polyynes: Application to the total synthesis of 15,16-dihydrominquartynoic acid. *Org. Lett.* **6**, 3601-3604, (2004).

3 Hoheisel, T. N. & Frauenrath, H. A convenient negishi protocol for the synthesis of glycosylated oligo(ethynylene)s. *Org. Lett.* **10**, 4525-4528, (2008).

4 Hoheisel, T. N. & Frauenrath, H. Glycosylated oligo(ethynylene)s via a Pd/Zn-mediated cross-coupling reaction. *Chimia* **63**, 208-210, (2009).

5 Ferrari, A. C. & Robertson, J. Resonant Raman spectroscopy of disordered, amorphous, and diamondlike carbon. *Phys. Rev. B* **64**, 075414, (2001).

6 Casiraghi, C., Ferrari, A. C. & Robertson, J. Raman spectroscopy of hydrogenated amorphous carbons. *Phys. Rev. B* **72**, 085401, (2005).

7 Kline, S. R. Reduction and analysis of SANS and USANS data using IGOR Pro. *J. Appl. Cryst.*, **39**, 895 (2006).